
MULTI-LAYERED REASONING FROM A SINGLE VIEWPOINT FOR LEARNING SEE-THROUGH GRASPING

A PREPRINT

Fang Wan
wanfang@ieee.org

Zheng Wang

Wei Zhang

Chaoyang Song*
songcy@ieee.org

October 21, 2025

ABSTRACT

Sensory substitution enables biological systems to perceive stimuli typically obtained by another organ, which is inspirational for physical agents. Multi-modal perception of intrinsic and extrinsic interactions is critical in building an intelligent robot that learns. This study presents a Vision-based See-Through Perception (VBSeeThruP) architecture that simultaneously perceives multiple intrinsic and extrinsic modalities via a single visual input in a markerless way, all packed within a soft robotic finger using the Soft Polyhedral Network design. It is generally applicable to miniature vision systems placed underneath deformable networks with a see-through design, capturing real-time images of the network’s physical interactions induced by contact-based events overlaid on top of the visual scene of the external environment, as demonstrated in the ablation study. We present the VBSeeThruP’s capability for learning reactive grasping without using external cameras or dedicated force and torque sensors on the fingertips. Using the inpainted scene and the deformation mask, we further demonstrate the multi-modal performance of the VBSeeThruP architecture to simultaneously achieve various perceptions, including but not limited to scene inpainting, object detection, depth sensing, scene segmentation, masked deformation tracking, 6D force/torque sensing, and contact event detection, all within a single sensory input from the in-finger vision markerlessly.

Keywords Multi-Modal Learning · Latent Representation · Tactile Robotics

1 Introduction

Sensory substitution [1] is a technique where one sensory modality is used to provide information typically perceived by another. Biological systems utilize visual cues to infer contact-based information, serving as inspiration for achieving multi-modal robotic perception [2]. In classical settings, such as the “Rubber Hand Experiment” [3], research has shown that humans can translate contact-based sensations into visual or auditory signals, enabling them to *see* through touch [4] or *hear* textures [5]. This concept naturally extends to understanding deformable interactions in both human and biological systems, where visual observations of deformations can infer underlying contact-based interactions and material properties [6]. This principle forms the basis of *Vision-Based Deformable Perception (VBDeformP)*, particularly in robotic manipulation, where the growing adoption of miniature vision sensors [7, 8] and robot learning methods [9, 10] are also notable. Accurately perceiving contact-based information is crucial for physical agents, such as robots, to effectively grasp and manipulate objects [11]. Leveraging visual cues of deformations offers a promising solution [12].

Robotics research has increasingly explored vision-based techniques to understand deformable objects [13] and their interactions with the object-centric environment [14]. Simultaneously achieving a comprehensive perception of the scene (i.e., object detection, recognition, and spatial understanding) and the touch-based interactions (i.e., surface texture, material properties, contact forces) during object manipulation with robots is an active research area [10].

*Corresponding Author.

However, achieving multi-modal perception within a single, compact visual input, especially when the sensor is embedded inside a soft robotic fingertip, poses a significant challenge [15]. The deformable interface between a miniature camera and the external environment plays a critical role in the accuracy and applicability of the system. Its design directly impacts the quality of both visual and contact-based information acquired, making it an emerging research area in tactile robotics [16]. An *ideal* system would be able to decouple the contact-based interaction gathered from the soft interface’s deformation from the miniature vision that also perceives the scene, all from a single visual input.

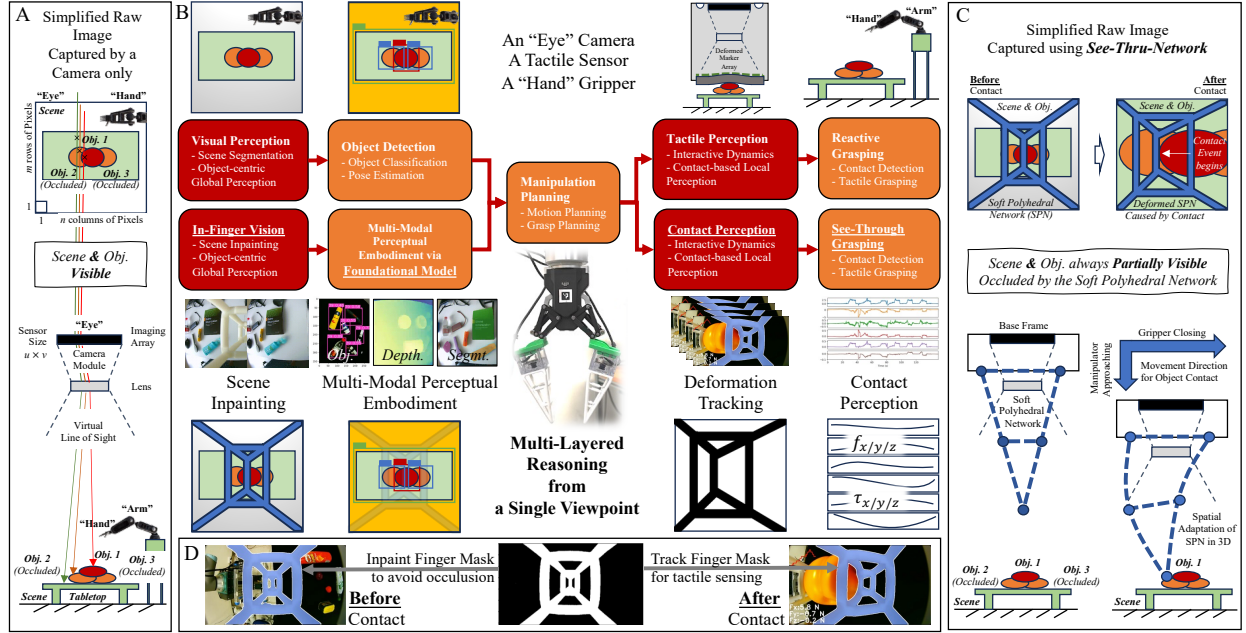


Figure 1: **Learning see-through grasping via multi-layered reasoning from a single viewpoint.** (A) A common setup for vision-based grasping. (B) Proposed pipeline in this work. (C) Grasping principle via See-Thru-Network. (D) Markerless representation via deformable mask tracking.

This work presents a *Vision-based See-Through Perception (VBSeeThruP)* architecture that enables multi-layered reasoning to learn reactive grasping from a single visual input behind a deformable network, serving as a markerless representation of fingertips, as shown in Fig. 1. The VBSeeThruP approach addresses the challenges of concurrently perceiving both finger deformation induced by contact-based interactions and rigid objects within the scene, all within a unified visual input for physical agents. For enhanced interactions with omni-directional adaptation of objects, we adopted the Soft Polyhedral Network (SPN) reported in recent research [17, 18], and further achieved markerless representations through multi-modal perception. The miniature vision captures real-time images of the SPN’s physical deformation during contact-based interaction while preserving partial information of the external scene. Before contact, a static SPN mask is used to inpaint the occluded scene via a brief “head-up” camera movement. Subsequently, video object segmentation of the SPN’s large-scale deformations provides markerless contact-based perception by estimating 6D forces and torques during contact. We demonstrate the viability of this approach through an ablation study and a reactive grasping task, further showcasing its potential to perform object detection, depth sensing, and scene segmentation once occluded regions are inpainted. This offers a unified solution that could streamline traditional hand-eye systems into a single in-finger vision sensor.

2 Related Works

Vision underpins robotic perception by enabling object detection, localization, and scene understanding [19, 20]. However, properties such as stiffness, friction, and mass are difficult to infer from vision alone [21, 22], calling for integration of alternative modalities.

2.1 Differentiating Vision-based Sensing and Perception

In robotics and cognitive science, sensing and perception are closely related but fundamentally distinct concepts, as summarized in Table 1. *Sensing* provides the foundational information required by robots or intelligent agents to interact

Table 1: A brief comparative summary of Sensing and Perception.

Aspect	Sensing	Perception
Data Type	Raw, unprocessed signals	Processed, interpreted information
Role	Data collection	Interpretation, understanding, and decision-making
Implementation	Primarily hardware-level	Primarily computational or cognitive algorithms
Complexity	Low-level, simpler	High-level, complex, involving learning or inference
Outcome	Raw sensor measurements	Meaningful representations or models
Example (Visual)	Camera pixels	Object detection, scene understanding
Example (Tactile)	Force/pressure readings	Recognizing object stiffness or shape

with the physical world. It refers to directly acquiring raw data from the environment using sensors. It is the preliminary stage of gathering signals or measurements. It typically involves hardware (e.g., cameras, microphones, force sensors, temperature sensors); produces unprocessed, quantitative, often noisy data; and measures passive or active physical signals without interpreting their meaning. For example, a camera captures pixel-level images, or a microphone records sound waves, which are typically considered forms of sensing. *Perception*, on the other hand, builds on sensing data, enabling robots to make informed decisions, adapt to new situations, and interact intelligently with the environment or humans. It involves processing, interpreting, and understanding sensory data to derive meaningful information or actionable insights about the environment or state. It often refers to the computational or cognitive processes involved in analyzing and interpreting sensor data, which include filtering, classification, recognition, inference, and decision-making tasks. Perception bridges the gap between raw sensing and actionable knowledge or behavior. For example, identifying objects within an image, recognizing human speech from audio signals, or estimating forces from tactile sensor data are generally considered forms of perception.

2.2 A General Classification of Vision-based Perception

An object-centric representation [23] leads to rigid-body assumptions or deformable interactions for visual understanding and reasoning, promoting robotic vision via *Vision-based Rigid Perception* (VBRigidP) and *Vision-based Deformable Perception* (VBDeformP), which are the leading approaches.

2.2.1 Vision-based Rigid Perception (VBRigidP)

VBRigidP methods traditionally assume rigid objects, leveraging tools such as Faster R-CNN [24] or YOLO [25] for detection, combined with pose estimation techniques (PnP, ICP) [26, 27] for manipulation tasks [28]. Although effective in structured industrial settings, VBRigidP and the rigid-object assumption become limiting for real-world scenarios involving deformable or partially deformable objects.

2.2.2 Vision-based Deformable Perception (VBDeformP)

VBDeformP extends beyond rigid bodies by tracking non-rigid shapes [29, 30]. Soft robotics, cloth manipulation, and surgical robotics applications exploit visual deformation cues to infer forces or material properties [31, 32]. By analyzing deformation in video, robots can estimate contact forces [33], plan tasks for large-scale cloth handling [31], or reconstruct object geometry [34], all without the need for specialized tactile sensors.

Emerging from VBDeformP is *Vision-based Tactile Perception*, which interprets tactile interaction by analyzing deformation images [35, 21]. Research has shown that detailed force and contact geometry can be inferred from images of a soft interface undergoing compression [36, 35], which can be further embedded into multi-fingered systems for object manipulation [37, 38]. Recent research has demonstrated tactile perception inferred at the *sensor* (e.g., normal and tangential forces [35], vibration [39], thermal [21], pretouch proximity [40]), *contact* (e.g., contact geometry [35], force and torque [18], contact events [41], material properties [42]), *object* (e.g., object localization [43], shape [33, 44], mass and dynamics [36], contents of containers [45]), and *action* (e.g., can be inferred from previous perceptual modalities for action selection and initialization, tactile feedback for low-level control, action termination, action outcome detection, and action outcome verification) levels [46], providing a cost-effective solution for tactile robotics [47].

It should be noted that the Vision-based Tactile Perception mentioned above is typically referred to as *Vision-based Tactile Sensing (VBTS)* in the computer vision and robotics literature. However, such terminology has caused some confusion among researchers in the cognitive science field, as the raw output signals obtained are camera pixels, and the subsequent tactile information is computationally processed to infer contact-based meanings for object manipulation. In addition, it could be argued that the tactile data collected using the VBTS method is not directly measured from compression readings regarding force or pressure on the interaction surface, but rather processed algorithmically based on the raw image pixels, making it more of a perception method than a sensing method. Without losing generality, we describe this approach as a subcategory of the VBDeformP method in this work, following the general review elaborated in Sec. 2.1.

2.2.3 Vision-based See-Through Perception (VBSeeThruP)

In this work, we introduce Vision-based See-Through Perception (VBSeeThruP), a novel approach that combines the benefits of both VBRigidP and VBDeformP to achieve multi-modal perception from a single visual input by reasoning about information obtained from different image layers during in-finger imaging. Cognitive science research on sensory substitution inspired our research in VBSeeThruP, as we can use a single visual sensing to infer multiple perceptual modalities by reasoning between various layers of information the camera captures. For example, our proposed VBSeeThruP architecture involves inferring contact-related information by tracking masked deformation from the See-Thru-Network (which is not limited to the Soft Polyhedral Network design exemplified in this work). The VBSeeThruP can also infer visual-related information after scene inpainting and the use of foundational models for a rich set of perceptual modalities in an object-centric scene. The combined effect is not achievable using VBRigidP or VBDeformP methods alone, and the resultant effect is enabled by introducing a See-Thru-Network in front of the in-finger camera. For example, when the network structure is 100% filled without see-through capabilities, it becomes equivalent to a VBTactileP (or VBTS) system. When it is 0% filled with complete see-through capabilities, it becomes equivalent to a VBRigidP system.

2.3 Multi-Modal Perception in Robotics with Vision

Combining vision and touch provides richer representations, improving classification [48], pose estimation [49], and in-hand manipulation [50]. This fusion is instrumental in cluttered or occluded environments [51, 52]. Pairing visual and auditory cues boosts performance in human action classification and material recognition [53, 54]. Multi-sensory attention mechanisms (vision, audio, touch) enhance performance for complex activities, such as pouring or packing [55, 56]. Recent multi-modal large language models (LLMs) combine visual perception with language-based reasoning, enabling zero-shot and few-shot policy learning [57, 58]. These systems exhibit stronger physical reasoning when additional modalities are incorporated [59, 60], widening opportunities for flexible, data-driven manipulation [61].

3 Proposed Methods

Our approach begins by denoting an image $\mathbf{X}_t \in \mathbb{R}^{m \times n}$ captured by a camera at timestep t . The m and n are the user-defined output settings for the image size, measured in the total count of pixel rows and columns. Depending on the camera selection, the i th row and j th column pixel entry of the image $x_{i,j,c,t}$ may contain the brightness intensity of a single channel for grayscale images ($c = 1$) or three channels in red, green, and blue (RGB) for color images ($c = 1, 2, 3$). Each pixel entry usually stores information in an 8-bit format, offering 256 conditions ranging from 0 to 255. Furthermore, we can add another data channel ($c = 4$) to the RGB image to include the transparency state of each pixel.

3.1 Markerless Design of the See-Thru-Network

Figure 2 is the Hand-Eye system adopted in this study, built with aluminum extrusion based on the DeepClaw workstation [62], housing a collaborative robot (UR10e from Universal Robots) on a pedestal and a tabletop in front covered by black fabrics. Although an “Eye” camera is fixed on the post shown in Fig. 2A, it is intentionally unplugged (therefore with a strikethrough) as we intend to implement visual perception of the scene using in-finger vision only behind a soft fingertip featuring a See-Through design using deformable materials. Figure 2B shows an enlarged view of the “Hand,” a two-fingered gripper (Model AG-160-95 from DH-Robotics) with its rigid fingertips replaced by the soft ones. Each soft fingertip contains a soft, omni-adaptive, markerless structure based on a variant of the Soft Polyhedral Network designs [63], mounted on a camera housing 3D-printed by UV-curable transparent resin (Somos WaterShed XC1112), where a miniature camera (Chengyue WX605 from Weixinshijie) is fixed inside.

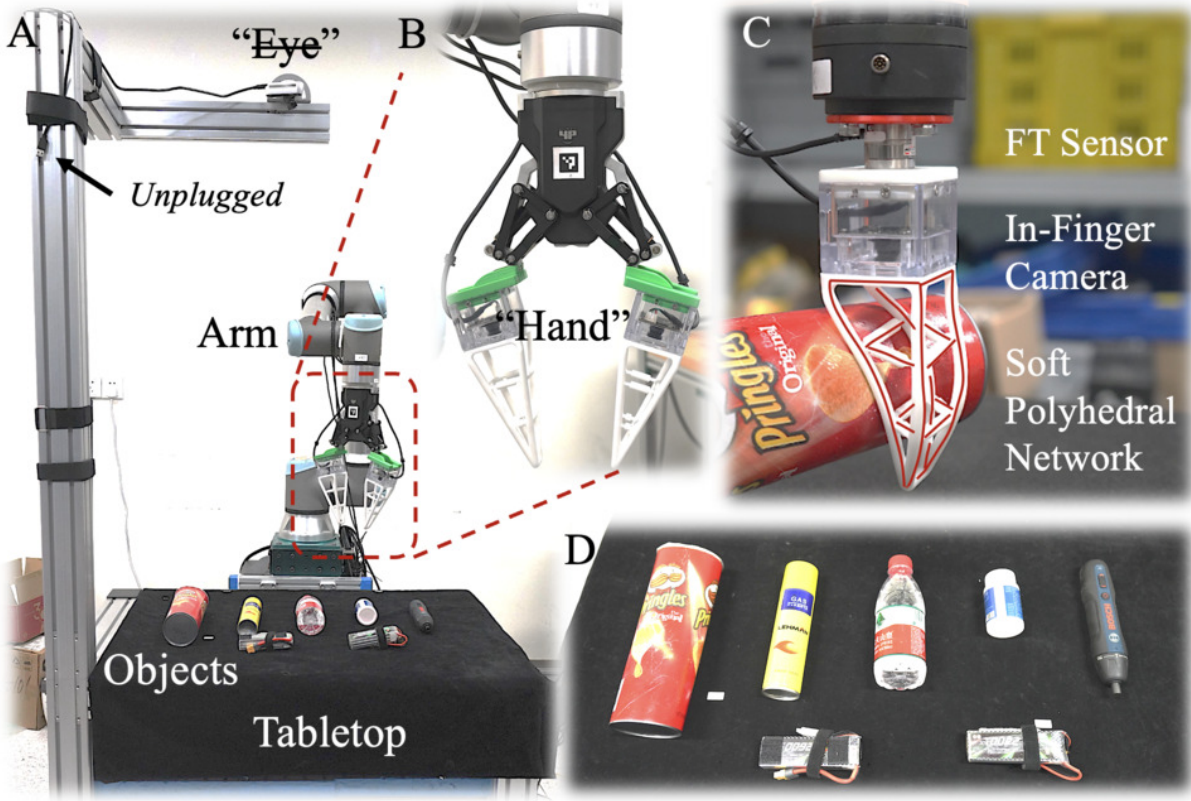


Figure 2: Platform setup as a hand-eye system.

As shown in Fig. 2C, the base plate can be customized to accommodate the installation of soft fingertips on force/torque (FT) sensors for testing or to use a gripper as a fingertip for soft and adaptive grasping. Figure 2D shows the objects used for testing in this study, including a Pringles Can from the Yale-Columbia-Berkley (YCB) object sets [64] and others commonly available at research labs, including a spray can, mineral water bottles filled halfway with water, a medicine bottle, a Bosche electrical screwdriver, pouch cell. Although both soft fingertips are functional, we only used the one whose viewing range partially covers the table at every frame throughout the following experiments.

3.2 Formalizing Multi-Modal VBSeeThruP

For an image $\mathbf{X}_t^{\text{InFinger}}$ taken by an in-finger vision camera, the resultant image is essentially the same as the general representation $\mathbf{X}_t^{\text{InFinger}} = \mathbf{X}_t$ reproduced in Fig. 3, with the ambient environment in gray. Suppose the in-finger camera is used for VBDeformP with an Illuminated Chamber (IC), the pixels of the image are related to the state of the soft membrane captured within the camera’s viewing range, containing zero information about the scene before contact begins [35, 21].

However, for an image $\mathbf{X}_t^{\text{STN}}$ taken by an in-finger camera for VBSeeThruP with a See-Thru-Network (STN), the resultant image contains the scene occluded by the Soft Polyhedral Network (SPN). We denote the image as $\mathbf{X}_t^{\text{STN}} = \mathbf{X}_t^{\text{STN}}$ if the SPN is in a Static State before any contact. We can add a hat to use the symbol $\widehat{\mathbf{X}}_t^{\text{STN}}$ to indicate a particular case if the scene is empty, captured as uniform pixel features. Here, the subscript timestep t is removed to simplify the representation. Since the valuable information captured in this image is purely regarding the SPN, one can add a transparency channel to obtain $\widehat{\mathbf{X}}_t^{\text{STN}}$, represented in white color in Fig. 3. Pixel data of the SPN is preserved in this added data channel, but the pixel data of the empty scene is set to transparent. Such an operation would produce a matrix $\widehat{\mathbf{M}}^{\text{STN}}$ that can be visualized as a Static Mask of the segmented SPN. Element-wise matrix multiplication of image $\widehat{\mathbf{X}}_t^{\text{STN}}$ and this Static Mask will produce masked image $\mathbf{X}_t^{\text{STN, Masked}}$. Note that performing the same operation using raw image $\mathbf{X}_t^{\text{InFinger}}$ will produce the same masked image instead. This also explains the SPN’s See-Through feature in the in-finger vision image occlusion process. The above process generally applies to scenarios when the SPN

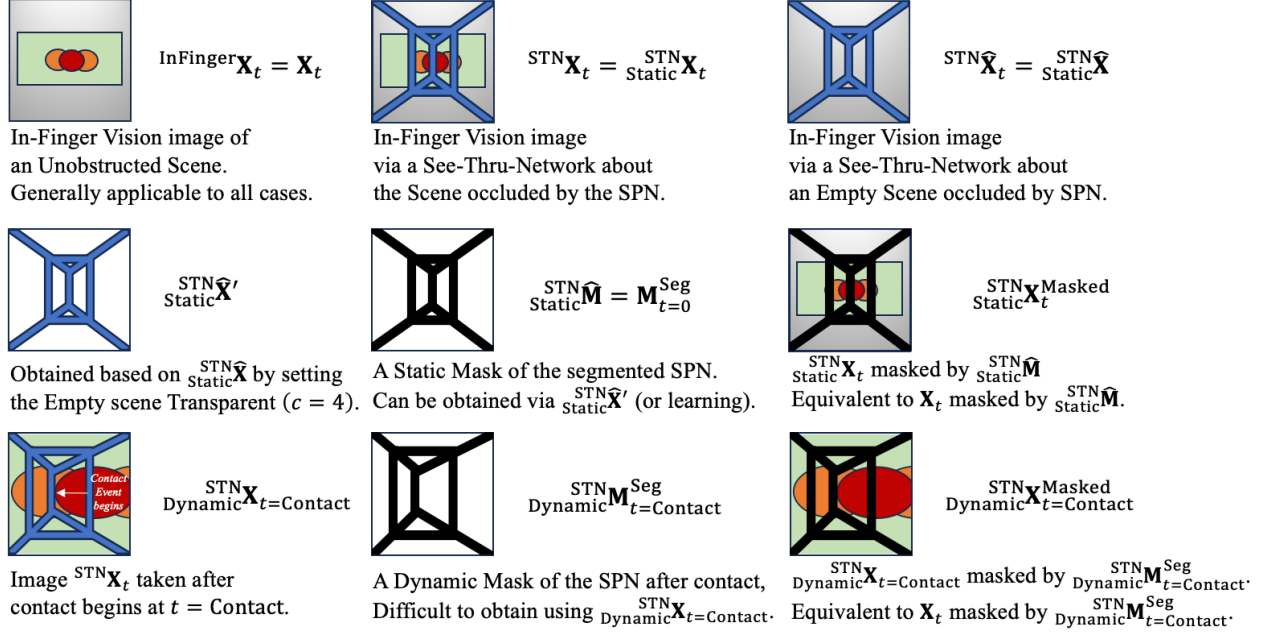


Figure 3: Multi-layered reasoning for VBSeeThruP based on the SPN’s See-Through design.

is in a Static State, meaning that no deformation is induced, as there is no contact event. One can use classical image processing techniques to obtain the above results.

However, the above process becomes complicated when contact events occur at $t = \text{Contact}$. On one side, the SPN enters a Dynamic State, exhibiting whole-body adaptive deformation during physical contact with the objects. On the other side, the See-Through scene also changes during contact, adding to the complexity of segmentation. The resultant image $\mathbf{X}_t^{\text{STN}}$ captured by the in-finger camera can be represented as $\mathbf{X}_{t=\text{Contact}}^{\text{STN}}$ when contact begins. Let us assume that the Dynamic Mask of the segmented SPN, $\mathbf{M}_{t=\text{Contact}}^{\text{STN, Seg}}$, could be obtained. Then, one should be able to obtain a masked image of the in-finger vision, $\mathbf{X}_{t=\text{Contact}}^{\text{STN, Masked}}$, by performing the same pixel-wise multiplication of $\mathbf{X}_{t=\text{Contact}}^{\text{STN}}$ using this Dynamic Mask. Similarly, this would be equivalent to applying the Dynamic Mask over an unobstructed in-finger vision image $\mathbf{X}_t^{\text{InFinger}}$. The challenge is that such a Dynamic Mask of the SPN will be intricate to obtain using classical methods, especially in cluttered scenes, which usually require advanced segmentation processing and feature engineering.

Using the symbols above, we formalize three research problems of this study for a generic scenario of reactive object grasping where both 1) scene-wise visual perception for object detection and 2) object-centric force/torque sensing are considered, as shown in Fig. 4 and Supplementary Video S1.

1. Throughout the whole grasping process, can we perform markerless, real-time, and large-scale deformation tracking of the interactive medium, i.e., the Soft Polyhedral Network, in both Static and Dynamic States to obtain a pixel-wise mask $\mathbf{M}_t^{\text{Seg}}$?
2. Before contact begins, can we reconstruct the unobstructed scene $\mathbf{X}_{t < \text{Contact}}$ from occluded in-finger images $\mathbf{X}_{t < \text{Contact}}^{\text{STN}}$ for visual perception, i.e., object detection, in a Hand-Eye system via in-finger vision only?
3. During contact-based physical interactions, can we infer high-precision 6D forces and torques $\mathbf{F}^T_{t \geq \text{Contact}}$ in a markerless way?

3.2.1 Markerless, Real-time, Large-Scale Deformation Tracking

The *first* problem is to enable markerless real-time segmentation tracking of the STN’s adaptive deformation during contact, which always covers a considerable image area with large-scale spatial deformations. This problem is equivalent to video object segmentation in computer vision. A significant challenge in addressing this problem is to efficiently manage the feature memory model, avoiding memory explosion while minimizing performance decay for long-term

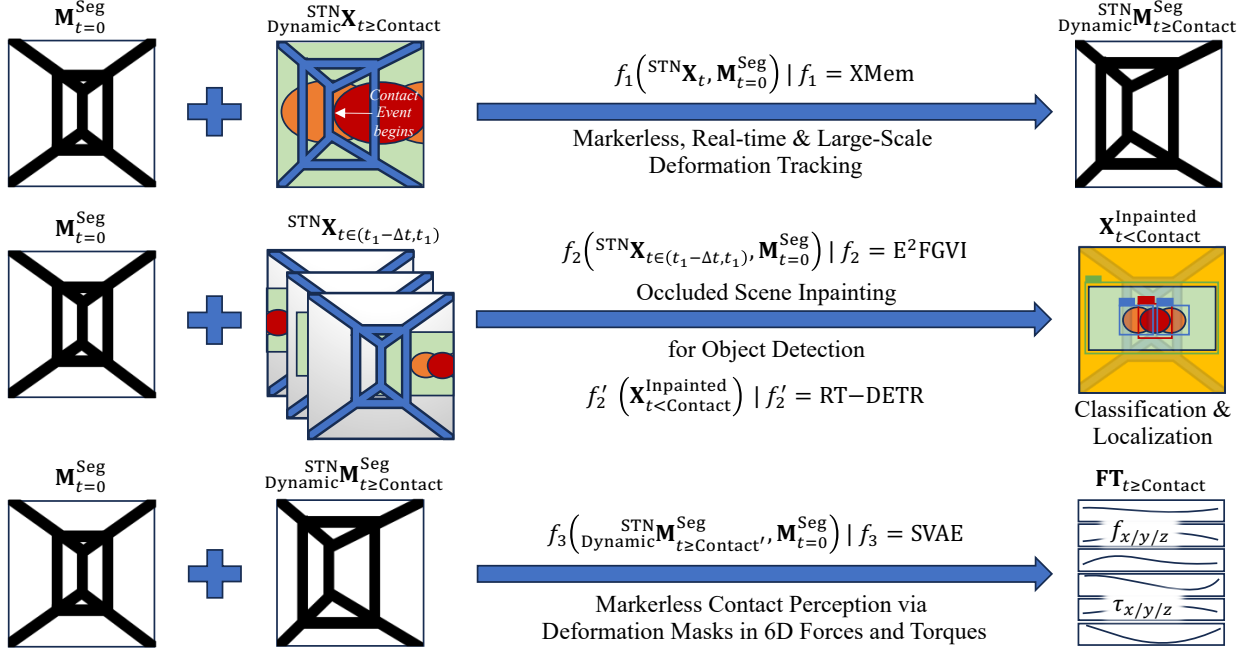


Figure 4: Formalizing three research problems for VBSeeThruP via a See-Thru-Network.

predictions. The latest development in a Unified Memory architecture, the XMem model, exhibits state-of-the-art performance on long-video benchmarking datasets [65].

In this study, we experimented with the XMem model for the in-finger video stream, as shown in Fig. 5, achieving a real-time implementation (30 Hz) of the STN’s large-scale deformation mask in a markerless way. This is realized by

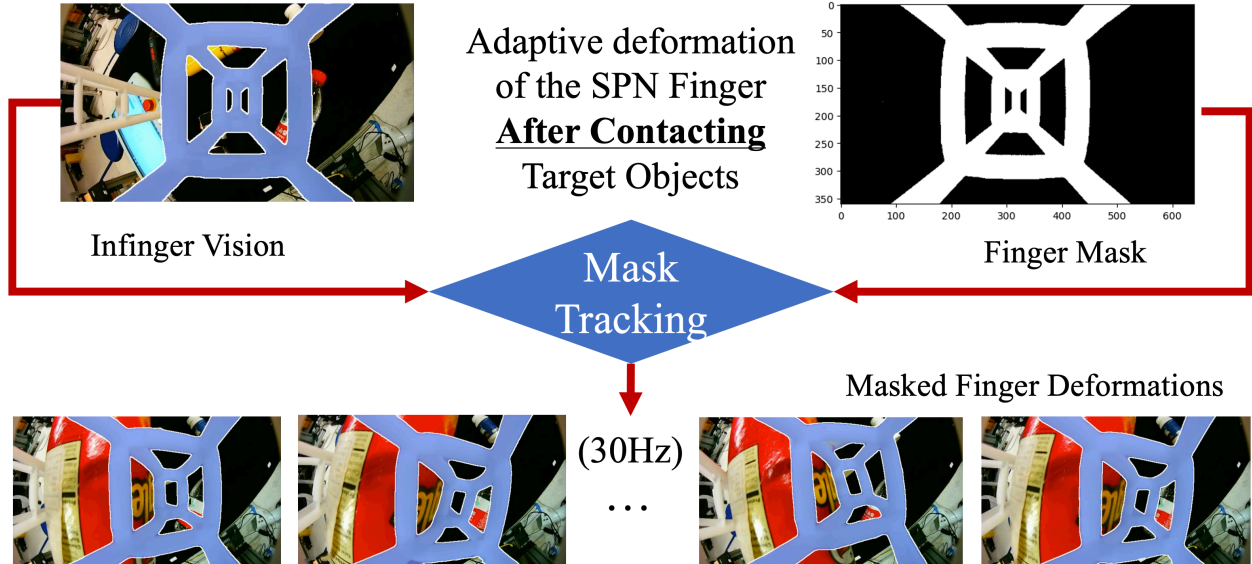


Figure 5: Markerless deformation tracking of STN mask.

using a Static Mask of the STN $\widehat{M}_{\text{Static}}^{\text{STN}}$ as the initial tracking target and the in-finger vision image $X_{\text{Dynamic}}^{\text{STN}}_{t \ge \text{Contact}}$ of the STN after contact. Before any contact event, this Static Mask remains the same and can be conveniently obtained manually or using advanced segmentation algorithms such as SAM [19]. The following formal representation addresses

the first research problem in Fig. 4.

$$\begin{aligned} {}^{\text{STN}}\mathbf{M}_t^{\text{Seg}} &= f_1({}^{\text{STN}}\mathbf{X}_t, \mathbf{M}_{t=0}^{\text{Seg}}), \\ f_1 &= \text{XMem}. \end{aligned} \quad (1)$$

We evaluated this mask segmentation over a test dataset of 1,000 samples, using the ground truth masks as a reference. The region (J) and boundary (F) measures [66] are 0.975 and 0.997, respectively, showing excellent reliability in tracking the soft finger’s spatial deformation masks in a markerless way. In applications, we found that XMem’s mask tracking of the STN’s deformation is not limited to the Dynamic States but also applicable to the Static States of the STN. We successfully implemented markerless and real-time deformation tracking of the STN whenever our proposed architecture is enabled, alleviating the need for artificial markers reported in previous VBDeformP literature. This process can also be used to detect the occurrence of a contact event, which will be further elaborated upon in the Results section.

3.2.2 In-Finger Visual Perception from Scene Inpainting

The *second* problem is reconstructing the scene using occluded images captured by the in-finger vision for visual perception, such as object detection, providing the equivalent capability to an external “Eye” camera. Due to the SPN’s See-Through feature, this problem becomes comparable to inpainting. Video inpainting has recently attracted significant research interest, where learning-based methods exhibit superior performances in filling in missing regions of a video with spatially and temporally coherent contents [67].

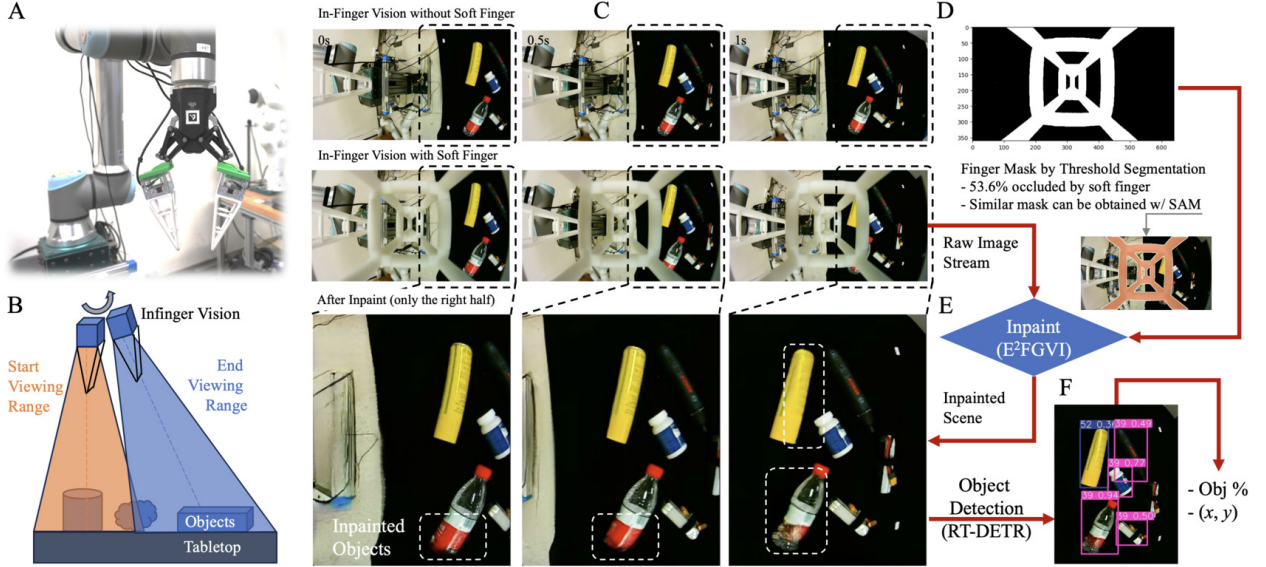


Figure 6: In-finger visual perception from occluded scene inpainting using VBSeeThruP.

We propose moving the soft finger shown in Fig. 6A to obtain redundant information about the scene by scanning sequential in-finger images from different poses of the same scene, accumulating sufficient visual features from the See-Through pixels to inpaint the occluded scene. Figure 6B illustrates a hard-coded head-up movement of the gripper for the in-finger camera to capture a short video ${}^{\text{STN}}\mathbf{X}_{t \in (t_1 - \Delta t, t_1)}$ in which its viewing range sweeps across the tabletop scene. The predefined movement can be linear above the robot’s working area with a fixed orientation. The first row of Fig. 6C shows the in-finger vision of the scene without attaching the STN, the second row shows the STN occluding the scene, and the third row shows the corresponding frames of the inpainted scene. Only the right half of the image with objects is inpainted for efficient processing. We ensured that all objects have been captured in at least one frame in the video, providing context for reconstructing frames where STN blocks objects.

We adopted the Flow-Guided Video Inpainting (E²FGVI) algorithm [68], a state-of-the-art algorithm for video inpainting. To facilitate the inpainting process, we obtain a Static Mask of the STN in Fig. 6D using threshold segmentation against a clean background, denoted as ${}^{\text{STN}}\mathbf{M}_{\text{Static}}$. Results show that the STN occludes about 53.6% of the in-finger image pixels. Alternatively, we can interactively obtain the same mask using the Segment Anything Model (SAM) by clicking for comparison in an actual scene [19]. Visual perception is usually performed before the contact event when $0 \leq t < \text{Contact}$ for an object manipulation pipeline. During this period, the STN is in a Static State, meaning that the

mask remains unchanged as the initial mask $M_{t=0}^{\text{Seg}} = \widehat{M}_{\text{Static}}^{\text{STN}}$. The E²FGVI algorithm has been reported with a high Structural Similarity Index (SSI) measure of 0.97 on two public datasets, YouTube-VOS and DAVIS, under stationary masks. Figure 6E shows the scene inpainting pipeline to implement the E²FGVI algorithm using in-finger video clip $\text{STN}\mathbf{X}_{t \in (t_1 - \Delta t, t_1)}$ and the STN's Static Mask $M_{t=0}^{\text{Seg}}$ to generate inpainted scene $\mathbf{X}_{t < \text{Contact}}^{\text{Inpainted}}$ with objects on the tabletop. This inpainting process is represented as

$$\begin{aligned} \mathbf{X}_{t < \text{Contact}}^{\text{Inpainted}} &= f_2(\text{STN}\mathbf{X}_{t \in (t_1 - \Delta t, t_1)}, M_{t=0}^{\text{Seg}}), \\ f_2 &= \text{E}^2\text{FGVI} \end{aligned} \quad (2)$$

The following focuses on implementing the reactive grasping task in Fig. 1. We use the Real-Time DEtection TRansformer (RT-DETR), a state-of-the-art object detection algorithm [69]. This object detection process is represented as

$$\begin{aligned} \{\%, (x, y)\} &= f'_2(\mathbf{X}_{t < \text{Contact}}^{\text{Inpainted}}), \\ f'_2 &= \text{RT-DETR}. \end{aligned} \quad (3)$$

The example shown in Fig. 6F verifies the feasibility of visual perception using an inpainted scene from in-finger vision occluded by the SPN, producing object classification (%) and bounding box center (x, y) that can be later used for grasp planning. Equations (2) and (3) are the formal representation of this implementation, addressing the second research problem in Fig. 4.

3.2.3 Markerless Contact Perception via a Deformation Mask

The *third* problem is to infer high-performing contact-based perception markerlessly using in-finger vision. This representation problem is usually resolved by adding artificial markers to the soft medium, which VBSeeThruP shares using either an Illuminated Chamber or a See-Thru-Network. Previous research has also explored fiducial markers within the STN, achieving high-performing proprioceptive perception, particularly when considering the STN's static and dynamic viscoelastic properties [18].

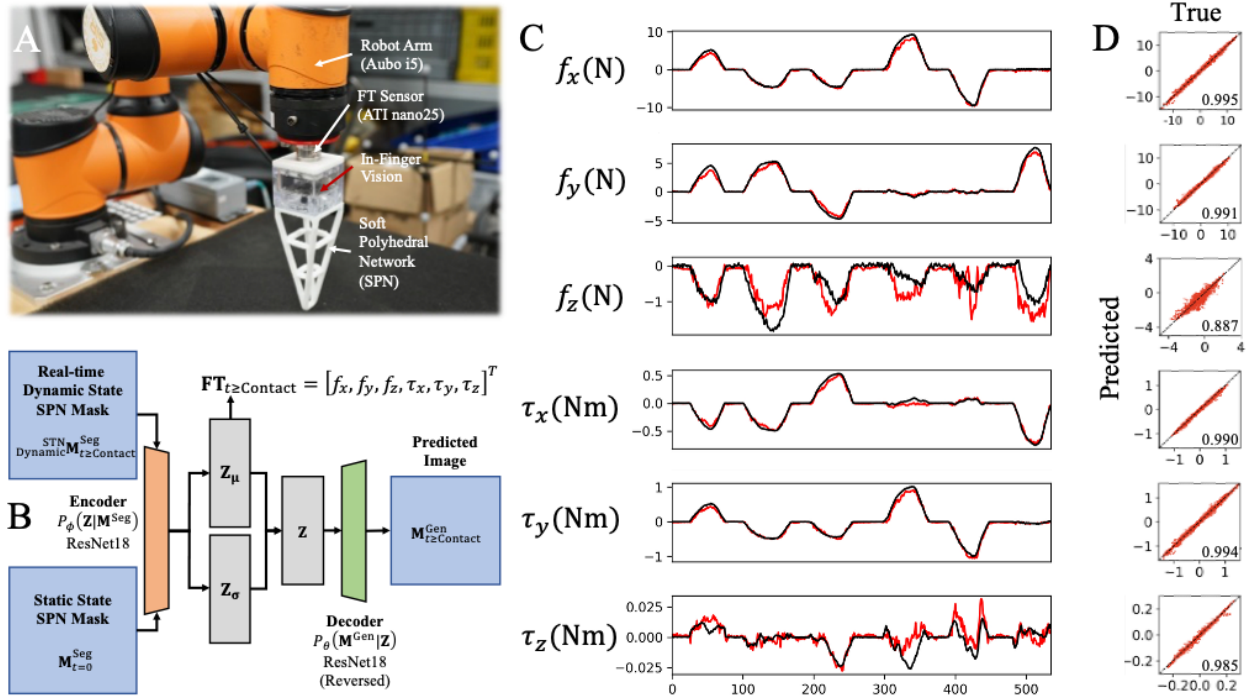


Figure 7: Experiment setup, the SVAE model, and results for 6D forces and torques estimated.

This study utilizes the STN masks in the Dynamic States, obtained from segmented tracking, as the model input to infer 6D forces and torques. We adopted the Supervised Variational AutoEncoder (SVAE) for this task, and Fig. 7A shows the experimental setup for collecting true labels of 6D forces and torques at the finger base using nano25 by ATI for calibration. The in-finger camera and FT sensor were connected to a laptop for data streaming. We collected 40,000

synchronized pairs of images and FT readings while manually compressing the two STN fingers from various directions and contact locations. We used an 8:2 train-valid split and trained the SVAE model for 50 epochs. To avoid excessive good validation scores due to the potential sample dependence, we separately collected a test dataset of 1,000 samples.

Figure 7B illustrates the SVAE model. The STN masks segmented in Dynamic States $\mathbf{M}_{\text{Dynamic}}^{\text{STN}} \mathbf{M}_{t \geq \text{Contact}}^{\text{Seg}}$ and the mask template $\mathbf{M}_{t=0}^{\text{Seg}}$ are fed to the ResNet18 encoder and decoder module to reconstruct the in-finger image $\mathbf{M}_{t > \text{Contact}}^{\text{Gen}}$. The latent space is set to 32 dimensions. At the same time, we design an auxiliary supervised regression task of the 6D forces and torques $\mathbf{F}\mathbf{T}_{t \geq \text{Contact}}$ simultaneously from the learned latent geometry representation. This leads to the formal representation of this implementation, addressing the third research problem in Fig. 4.

$$\{\mathbf{F}\mathbf{T}_{t \geq \text{Contact}}, \mathbf{M}_{t \geq \text{Contact}}^{\text{Gen}}\} = f_3(\mathbf{M}_{\text{Dynamic}}^{\text{STN}} \mathbf{M}_{t \geq \text{Contact}}^{\text{Seg}}, \mathbf{M}_{t=0}^{\text{Seg}}),$$

$$f_3 = \text{SVAE}. \quad (4)$$

Table 2: Evaluation of the Supervised Variational AutoEncoder (SVAE) model for 6D forces and torques.

MAE Datasets	Force (N)			Torque (Nm)		
	f_x	f_y	f_z	τ_x	τ_y	τ_z
Validation	0.241	0.212	0.14	0.024	0.027	0.005
Test	0.328	0.283	0.24	0.027	0.036	0.005

The overall loss comprises reconstruction loss, Mean-Squared Error (MSE) loss for force and torque prediction, and Kullback-Leibler divergence. The average time for a single inference is 1.9 milliseconds on an NVIDIA GeForce RTX 3080 Ti Laptop GPU. The Mean Absolute Errors of the validation and test datasets are reported in Table 2, indicating good generalization of the learned model.

Figure 7C compares the test dataset’s prediction and ground truth in time series. Figure 7D shows the scatter plot of such comparison in the validation dataset with excellent R^2 scores over 0.985 in all components except f_z . The relatively weak perforce in f_z is due to the limited adaptability along the z -axis. We also evaluate the resultant force in the xy plane and find that the mean magnitude and orientation error are 0.286 N and 2.6 degrees, respectively.

3.3 Ablation Study

This section presents an ablation study demonstrating how VBSeeThruP contributes to a multi-modal grasping pipeline without requiring additional or external devices. In particular, we investigate how in-finger vision and soft compliance from VBSeeThruP improve the reliability and generalization in a pick-and-place scenario. Please refer to Supplementary Video S2 for further details.

We begin by performing depth detection of table height relative to the robot base frame. Specifically, we tilt the gripper vertically downward until it contacts the table with a force of 0.5 N. Next, we calibrate the hand-eye in the desktop’s 2D plane to obtain the perspective transformation between VBSeeThruP’s in-finger camera space and the robot base frame.

For the calibration process, we place four oranges (or any objects of similar size) on the table and detect their centers $\{(u_i, v_i) \mid i = 1, \dots, 4\}$ in the image plane using YOLO11 [70] (see Fig. 8A). An operator then manually bends the soft finger (for horizontal x - y movement) to position the gripper over each orange. Once the gripper is centered above an orange, we record the corresponding world coordinates $\{(x_i, y_i) \mid i = 1, \dots, 4\}$ in the robot base frame by twisting the soft finger (clockwise and counter-clockwise to mark the start and end of data recording). The overall setup is shown in Figs. 8B&C, and a full demonstration is provided in the supplementary video. Notably, our method solely relies on VBSeeThruP for depth detection, whereas a typical solution would require an external depth camera.

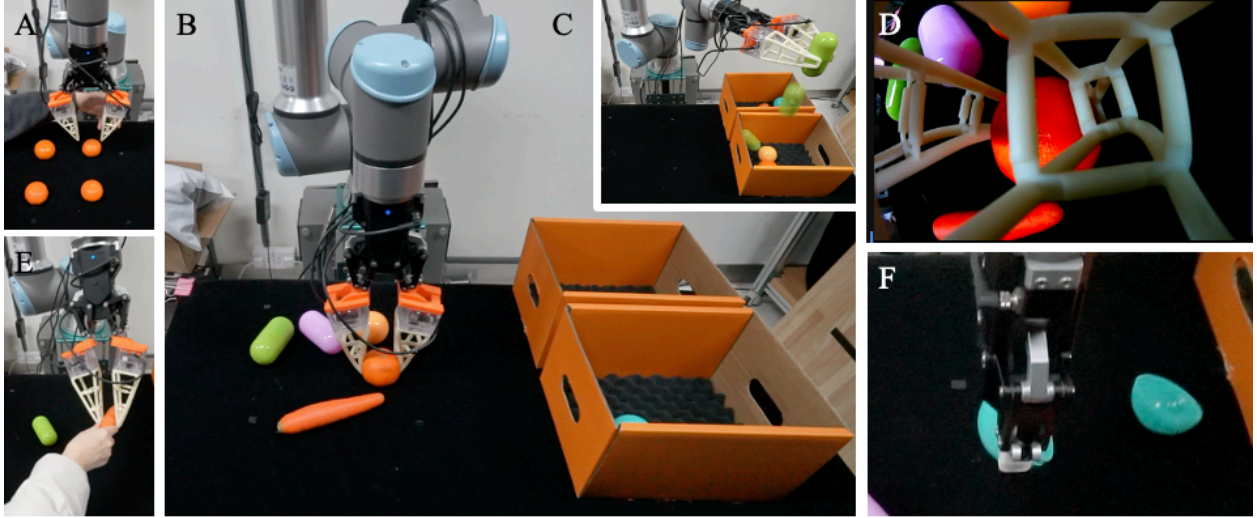
We employ the following control policy to facilitate intuitive robot teaching:

$$v_i = \begin{cases} 0, & |f_i| < 1, \\ V_{\max} (f_i - 1)/4, & 1 \leq |f_i| \leq 5, \\ V_{\max}, & |f_i| > 5, \end{cases} \quad i \in \{x, y\}, \quad (5)$$

where v_i denotes the translational velocity in the i -th direction, and f_i the corresponding finger deformation. For convenience, we also define two additional commands triggered by the torque τ_z :

$$\text{command} = \begin{cases} \text{Record current position,} & \tau_z > 0.2, \\ \text{Exit program,} & \tau_z < -0.2. \end{cases} \quad (6)$$

Using the pairs of recorded images and robot-world coordinates, we compute the homography matrix H , enabling transformations between the in-finger vision space and the robot base frame.



G	Method	Ablation Tasks					
		Rate of Objects being Placed in the Box			Rate of Successful Weight Classification		Human Disturbance
	SPN Only	4/6	1/6	1/6	Not Applied		Not Applied
	SPN + In-Finger Vision	5/6	4/6	5/6	Not Applied		Applied
	SPN + In-Finger Vision + Inferred 6D Force/Torque	6/6	6/6	6/6	6/6	5/6	6/6
	Rigid + External Vision + Wrist Force/Torque	4/6	4/6	3/6	4/4	4/4	2/3

Figure 8: **Experiment setup and results of the ablation study.** (A) Hand-eye calibration setup for perspective transformation; (B) Picking objects with similar shapes but different weights; (C) Weighing objects for sorting, then placing them into corresponding boxes; (D) Adaptive grasping of objects of varying sizes without specifying the fingers' closing width; (E) External disturbance for the carrot by intentionally removing it from the gripper; (F) Object damaged by a rigid finger; (G) Summary of the ablation study results.

3.3.1 Abalation Experiment Setup

We conducted a pick-and-place sorting task with six objects sharing similar geometry but different weights, including 1) Two hollow plastic balls (6 cm radius): one empty and one filled with a 100 g metal block; 2) Two plastic capsules (5 cm radius, 10 cm length): one empty and one containing 100 g of jelly balls; 3) One orange (6.7 cm radius, 131 g); and 4) One carrot (3.1 cm radius, 122 g).

We tested four different ablation conditions:

1. **SPN Only:** We use the SPN's adaptive grasping with no in-finger vision or FT. The grasp position (x, y) and rotation r are randomly generated, and the gripper's closing width is fixed at 1.5 cm for all objects.
2. **SPN + In-finger Vision:** We augment the SPN with soft fingers' in-finger vision for scene inpainting and YOLO11-based [70] object localization. The grasp width remains fixed at 1.5 cm.
3. **SPN + In-finger Vision + Inferred 6D FT:** Besides in-finger vision, the system leverages the soft finger's deformable sensor for estimating 6D forces and torques. We use reactive grasp control to maintain a constant grasp force of 3 N ($f_x = 3$ N) and continuously monitor grasp force during transport. If the force drops to zero (e.g., due to an external disturbance), the system will attempt to regrasp.

4. **Rigid + External Vision + Wrist FT:** We replace soft fingers with the original rigid fingertips and rely on an external camera for object localization. The gripper width is set based on the object’s oriented bounding box, and wrist-mounted force/torque sensing on the UR10e provides feedback.

We evaluate each setup on three aspects:

- **Pick-and-place success:** The ability to pick objects from the tabletop and place them into a designated box.
- **Weight classification before placement:** In the third ablation condition, we aggregate the two f_y readings from each soft finger and estimate the object mass m_{obj} as

$$m_{\text{obj}} = \frac{|f_y^1| + |f_y^2|}{9.8}. \quad (7)$$

We use the f_z reading from UR10e’s wrist FT sensing in the fourth ablation condition.

- **Recovery from human disturbance:** We manually remove the carrot from the gripper during the transport (Fig. 8D) to test whether the robot detects the event and regrasps successfully.

3.3.2 Ablation Results and Discussion

Each experiment scenario was repeated three times. We observed that even in the most straightforward configuration (**SPN Only**), objects could often be picked without damaging them or triggering safety stops, owing to the compliance offered by the soft finger. For example, the soft, deformable fingertips are easily adapted to objects from different angles, as shown in Fig. 8E (grasping an orange from the side with bending and twisting deformations). In contrast, using the original rigid fingertips without carefully specifying object dimensions frequently caused collisions and emergency stops.

When **in-finger vision** was added (**SPN + In-finger Vision**), the grasp location (x, y) and orientation r were derived from YOLO11, significantly improving the success rate over random grasps. Nevertheless, the lack of force feedback made the system less robust under disturbance, causing the robot to fail regrasp attempts in several trials (shown in the supplementary video). In one case, the fingertip was misaligned and exerted excessive force on a plastic ball, causing it to slide out of the gripper.

The configuration with **SPN + In-finger Vision + Inferred 6D FT** overcame these issues using 6D force/torque estimates for closed-loop grasping. As a result, it achieved a 100% success rate under the same disturbance conditions. It also enabled weight classification to differentiate between empty balls and allowed the system to adaptively regrasp objects if an object fell was detected.

Comparatively, the **Rigid + External Vision + Wrist FT** setup offered an unobstructed camera view of the workspace but lacked the compliance of soft fingers. Small errors in object detection or hand-eye calibration frequently led to inappropriate grasp forces, sometimes resulting in damaged objects (Fig. 8F) or failed grasps. All experiment outcomes are summarized in Fig. 8G.

The results indicate that VBSeeThruP’s in-finger vision and compliance significantly improve the success rate and robustness of pick-and-place tasks over alternative setups. The robot achieves reliable picking, weight classification, and effective regrasping after disturbances without requiring external cameras or specialized sensors. Even when paired with an unobstructed external vision system, rigid fingers are more likely to cause failure or exert excessive force, underscoring the advantage of soft fingers with built-in sensing.

4 Results and Discussion

4.1 Learning Reactive See-Through Grasping

This section demonstrates the application of the proposed architecture for learning reactive see-through grasping, shown in Fig. 1, in an object-picking task, shown in Fig. 2, using VBSeeThruP with a See-Thru-Network to achieve object detection and 6D forces and torques for reactive grasping simultaneously. Please refer to Supplementary Video S3 for a video demonstration.

The task begins with visual perception of the scene using the VBSeeThruP for object classification and localization. During the first attempt, the gripper will attempt to pick up the object at the center of the bounding box and a fixed rotation angle θ_0 and depth z_0 perpendicular to the table. We intentionally used a simpler algorithm without the optimal orientation to test reactive grasping.

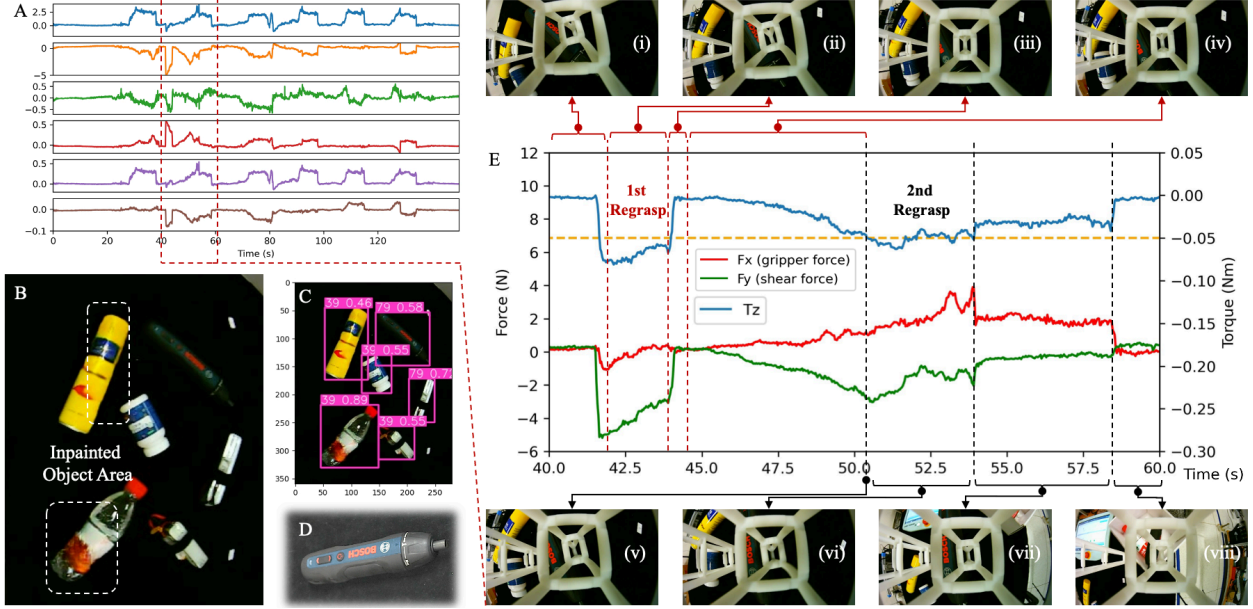


Figure 9: **VBSeeThruP demonstration for learning reactive see-through grasping.** (A) Time series 6D forces and torques were recorded, where the red dashed box marks the reactive grasping process for the Bosche electrical screwdriver. (B) Inpainted scene via in-finger vision, where the white dashed boxes are the inpainted portions of the scene and objects. (C) Visual perception of the inpainted scene via object detection. (D) The Bosche electrical screwdriver that requires reactive grasping. (E) A detailed plot of the 6D forces and torques for reactive grasping of the Bosche electrical screwdriver and multiple screenshots of in-finger vision.

While approaching the initial grasping pose, VBSeeThruP detects if it has contact with the object by inferring real-time 6D forces and torques based on the finger’s whole-body deformation. Due to the network design, the finger can deform in a twisted manner to generate torque about the z -axis. When τ_z is detected to be larger than 0.05 Nm, the object orientation is severely different from the gripper’s initial pose, suggesting a less ideal grasping that can be optimized through regrasping by turning the wrist reversely to reduce τ_z for an enhanced adaptation and grasping robustness. When τ_z is within the threshold, the gripper closes its fingers until the gripping force f_x reaches the predefined maximum gripping force of 3 N. Then, the gripper lifts the object and drops it into the placement box. We repeated the process until all five objects were cleared from the table.

Figure 9A shows the recorded 6D FT sensing data using VBSeeThruP for the table-cleaning task, where the six peaks in f_x indicate the grasping of the six test objects. The inpainted scene using VBSeeThruP is shown in Fig. 9B, where the occluded regions are inpainted with coherent details, and the overall contours of the objects are well reconstructed. Although some surface textures generated are blurry, they are sufficiently accurate to reflect their actual textures. Figure 9C shows object detection results based on the inpainted scene, showing bounding boxes for each detected object. The most exciting result is the regrasping of the Bosche electrical screwdriver shown in Fig. 9D. By inspecting the detailed FT history in Fig. 9A, we identified two regrasping attempts of the Bosche electrical screwdriver performed by the VBSeeThruP with the soft fingers.

Figure 9E is an enlarged view of the red dashed box region in Fig. 9A. When we performed the first grasping attempt in Fig. 9E(i), the finger detected the τ_z greater than 0.05 Nm in the negative direction. Then, in Fig. 9E(ii), the first reactive grasping begins rotating the gripper about the z -axis to reduce τ_z . During the process, the screwdriver suddenly turns to another side and temporarily loses contact with the finger in Fig. 9E(iii), as both f_x and f_y dropped to 0 suddenly. In Fig. 9E(iv), the gripper keeps closing, attempting to detect contact with the screwdriver again to keep increasing τ_z for an enhanced grasping pose. Next, the soft finger detected contact with the screwdriver again in Fig. 9E(v), marking the starting point of the second reactive grasping attempt. The soft finger repeated the same procedure by performing the second reactive grasping in Fig. 9E(vi), rotating the gripper about the z -axis until the detected τ_z is reduced towards 0. As a result, the screwdriver is secured between the fingers and moved toward the drop box in Fig. 9E(vii). Finally, the soft finger dropped the screwdriver with forces and torques approaching zero, as shown in Fig. 9E(viii).

4.2 Towards a Multi-Modal Soft Touch vis VBSeeThruP

Here, we discuss the extended modalities perceivable via our proposed architecture in Fig. 1, providing an intuitive understanding of the three research problems illustrated in Fig. 4 that aim to achieve multi-modal perception with a soft touch. Please refer to the following sections and Supplementary Video S4 for further details.

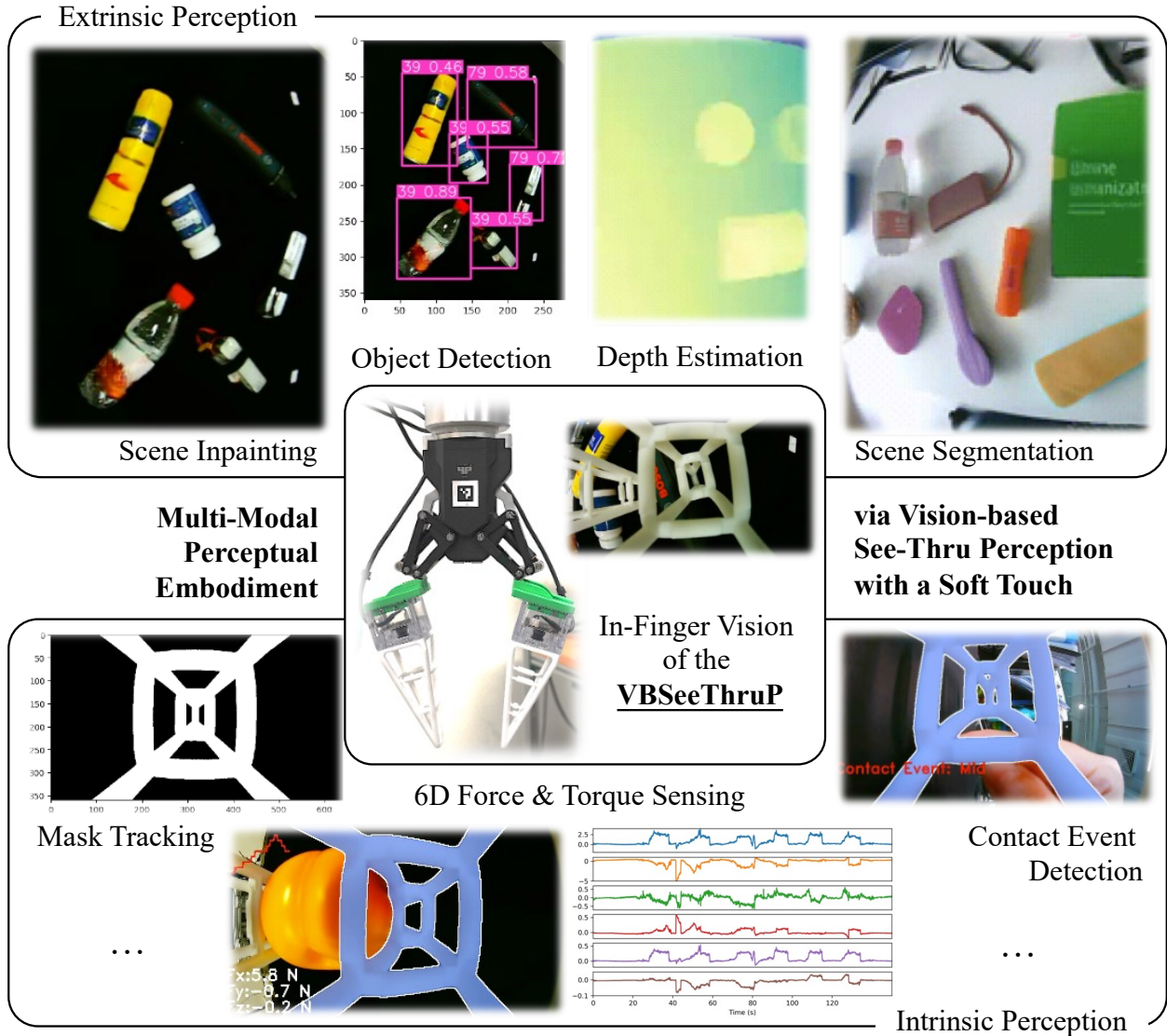


Figure 10: Towards multi-modal perceptual embodiment.

Using a single sensory input from the in-finger vision featuring See-Thru-Networks, we present a multi-modal approach towards robotic perceptual embodiment via VBSeeThruP with a soft touch, as shown in Fig. 10. Our proposed architecture can be generalized to further generate various outputs for extrinsic perception, including inpainted scenes, object detection, depth sensing, and scene segmentation. For intrinsic perceptions, we demonstrate the implementation of our architecture, which generates outputs including masked deformation tracking, 6D FT sensing in real-time with high accuracy, and contact event detection. Further expansion to other intrinsic or extrinsic modalities can also be implemented.

4.2.1 Markerless, Real-Time & Large-Scale Deformation Tracking

VBSeeThruP generically describes a class of soft robotic fingers/fingertips that involves a See-Thru-Network with in-finger vision as a design feature. The See-Through feature enables the in-finger vision to simultaneously capture visual features from the finger structure and the external environment. In this study, the See-Thru-Network is implemented using the Soft Polyhedral Network. However, researchers have a wide range of design choices to customize the soft interface as needed, as long as the resultant image contains sufficient details from both the finger structure and the external environment. The resultant performance is determined by the level of detail when extracting the soft structure’s deformation and the reusable information left to reconstruct the scene.

Algorithmic development in video object segmentation is a well-researched field that enables convenient implementation of this capability for See-Thru-Networks with in-finger vision. The 30 Hz mask tracking implemented in this study is sufficiently high to enable real-time processing for robotics without adding to the computational burden of the robotic systems. Future research to allow a higher mask tracking bandwidth is preferred to increase the upper bound in collecting sensory feedback (towards 1 kHz) from in-finger vision, requiring higher-framerate miniature cameras and high-performance mask tracking algorithms for more challenging robotic applications. The quality of mask segmentation at this step generally determines the maximum performance one can expect from the VBSeeThruP architecture in multi-modal perception. The solution to this problem provides the foundation for implementing suitable robotic solutions to address the second and third research problems.

4.2.2 Multi-Modal Visual Perception of the Occluded Scene via In-Finger Vision

An intuitive understanding of the second research problem is whether we can utilize in-finger vision for environmental perception, which is inherently multi-modal, thereby eliminating the need for an external camera in modern robot workstations.

Using in-finger vision for environmental perception is counterintuitive. Having an *Eye* camera fixed to the robot base is generally perceived as bio-inspired by humans or most living creatures, where visual organs are on the body for environmental perception. This is also a feature shared by most robotic systems. After masked segmentation of the See-Thru-Network, the original image becomes fragmented. Still, it could be alternatively *repaired* using inpainting, a highly active field of research in computer vision and widely adopted practice throughout history. A direct result of inpainting the in-finger vision is the reconstruction of the scene, producing visual perceptual capabilities *almost* precisely as a typical Eye camera. It should be noted that the inpainting technique is computationally intensive, requiring high-performing hardware and long processing time, neither of which is ideal for robotic applications. In this study, we added an extra head-up motion during motion planning to collect an extra 1-second video clip for inpainting as a trade-off.

In the sections above, we demonstrated object detection using inpainted images from in-finger vision. Here, we showcase the performance of achieving other modalities, such as depth sensing and scene segmentation, using the inpainted images, which are also widely used in modern robotics. In principle, robotists can reuse the inpainted images for any desirable extra modalities as needed, just as in a computer vision problem, making the VBSeeThruP architecture a generic solution for robotics, where constraints in hardware cost and computational power are significant considerations.

Depth Sensing We estimated monocular depth based on the inpainted scene as proof of concept. We compared the reconstructed scene depths from both the in-finger camera and a camera with an unobstructed view of the robot’s working space. In this experiment, ten objects with various shapes and colors (milk powder can, tape, rubber ball, strawberry, glue, plum, glue stick, power drill with a packaging box, and drill toolkit) were placed on the tabletop. The robotic arm swept across the tabletop from left to right and returned to the starting point with a fixed orientation while the in-finger camera inspected the objects. We recorded both the in-finger and unobstructed videos by removing the SPN from the gripper. The former was further inpainted by the E²FGVI algorithm. The inpainted and unobstructed videos are then fed to the Depth Anything V2 model [71] to obtain the depth estimations. The pixel-wise estimations provide relative depth values, offering helpful information on the relative poses of objects on the table. Hence, instead of comparing the actual values of the depth map, we adopt the structural similarity index (SSI) to evaluate the similarity between the depth map reconstructed from the inpainted view and that from the unobstructed view.

As shown in Fig. 11A, the index varies between 0.71 and 0.95 with an average of 0.87. Figure 11B-D shows three snapshots of in-finger vision, the depth map estimated from the inpainted view, and the SSI map. Low SSI values prominently occur at the objects’ edges, where depth estimation is inherently more challenging.

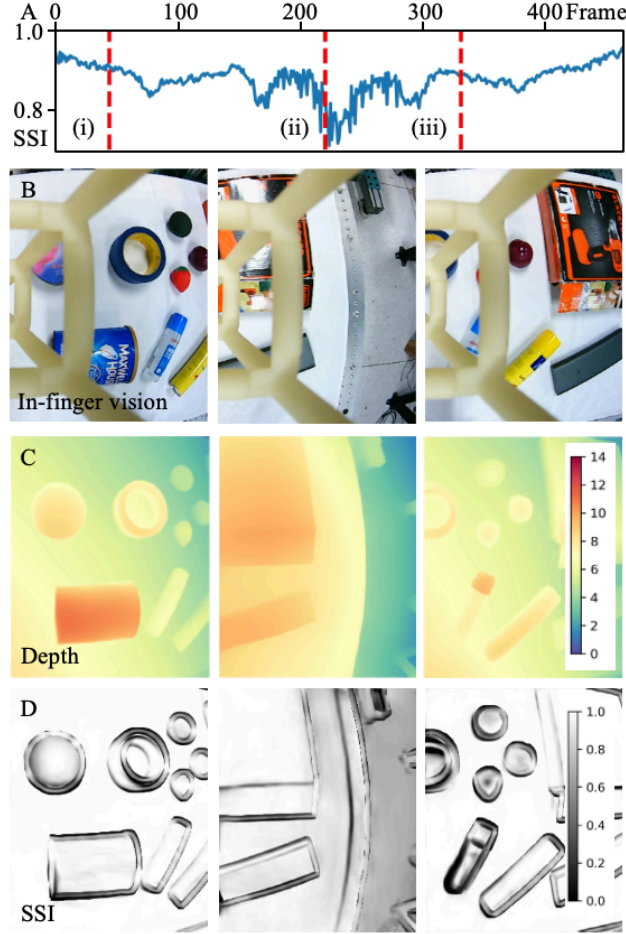


Figure 11: **Depth estimation by seeing through the finger after inpainting.** (A) Time series of Structural similarity index (SSI) measures between depth estimations from the inpainted and unobstructed views. The red lines marked in (i), (ii), and (iii) indicate the snapshot frames of (B) in-finger vision, (C) reconstructed depth map, and (D) SSI map.

Scene Segmentation Furthermore, we explored the feasibility of multi-object segmentation on the inpainted scene using the latest Segment Anything Model 2 (SAM2) [72]. We tested on the same scene described in the depth estimation task.

As shown in Fig. 12A, segmentation on the inpainted view achieves satisfactory performance with J measurement ranging between 0.64 and 0.87, which is 16% lower than the performance of segmentation on the unobstructed view on average. An interesting observation occurred in the segmentation of object 9 (a power drill with a packaging box), where the inpainted view performed better than the unobstructed view. Further frame-by-frame examination shows that the worst segmentation in the unobstructed view was caused by the intense surface reflection of the drill’s packaging box, and in some frames, SAM2 failed to segment object 9. On the contrary, SAM2 successfully tracked object nine in the inpainted view. The snapshots of the unobstructed and in-finger vision and segmentations of the inpainted scene at two different times are shown in Figs. 12C&D.

Multi-Modal & Markerless VBSeeThruP

An intuitive understanding of the third research problem is whether we can utilize in-finger vision with a soft finger to achieve high-performing, multi-modal perception in a markerless manner. Similar capabilities have been widely researched in the past literature, but the involvement of artificial markers remains a challenge among the current solutions [73, 74, 75, 76]. In this study, a by-product while addressing the first research problem is the real-time, pixel-wise segmentation of the See-Thru-Network’s mask M_t^{Seg} throughout the implementation of the VBSeeThruP architecture. Visual features from this mask provide a robust sensory input to infer FT information once a calibration dataset is obtained against commercial FT sensors for model training.

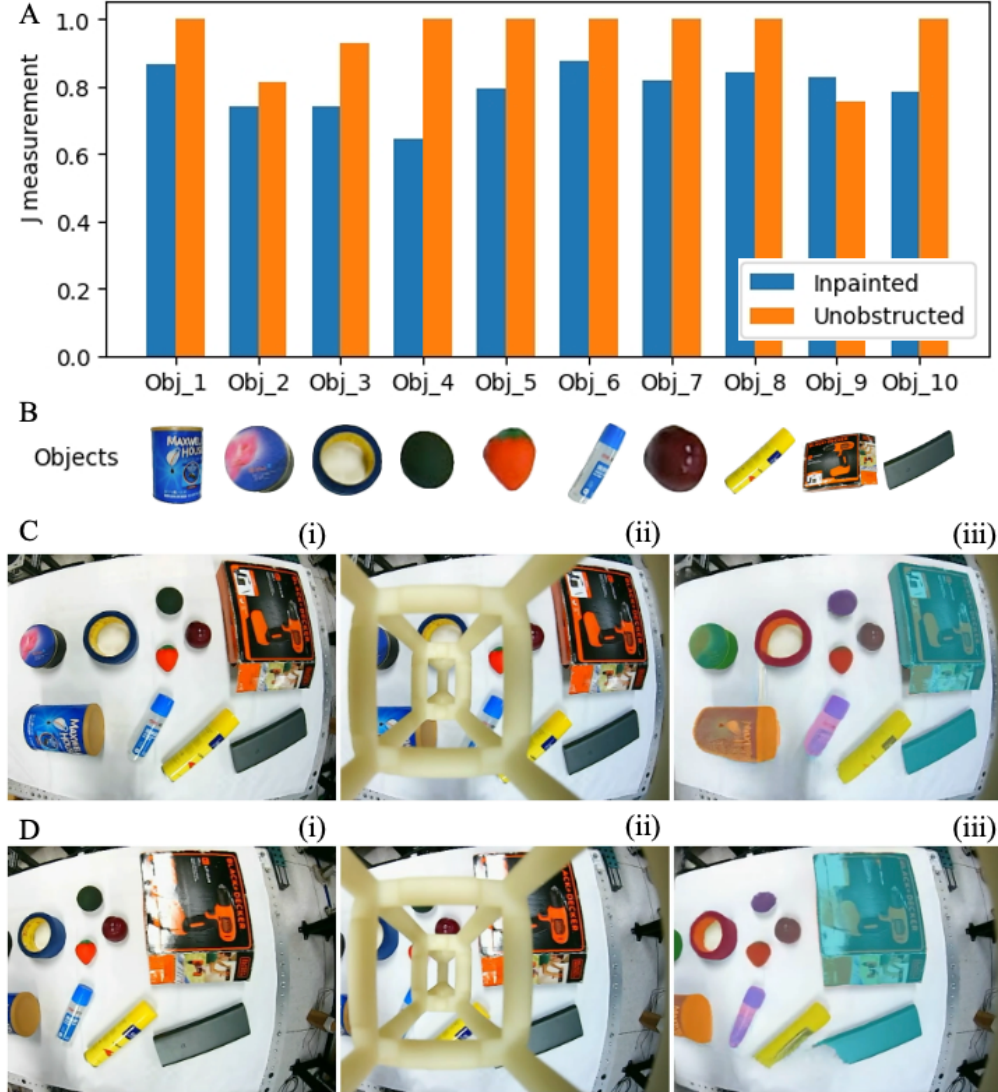


Figure 12: **Segmentation by seeing through the finger.** (A) The performance comparison of SAM2 on the inpainted and the unobstructed view of ten objects, measured by intersection over Union (Jaccard index); (B) Ten objects with various shapes and colors: milk powder can, tape, rubber ball, strawberry, glue, plum, glue stick, power drill with a packaging box, and drill toolkit; (C) Snapshot of the unobstructed and in-finger vision and the resultant segmentation of the inpainted scene; (D) A different snapshot similar to (C).

While it is reasonable to use simpler neural networks, we adopted a generative approach in this study and utilized the Supervised Variational Autoencoder (SVAE) to address this problem. The latent variables obtained from SVAE are a powerful tool for inferring various sensory modalities, requiring minimal disruption to the overall computation. Besides the 6D FT, we demonstrate a simple implementation to infer the contact event on the soft finger. Recent research also shows promising results in proprioceptive shape reconstruction [17], contact point estimation [34], and tactile perception using in-finger vision [18] with the soft polyhedral network used in this study, which could be further implemented using the deformation mask tracked in this study.

Contact Event Detection In previous work where the complex deformations of SPN are physically encoded into a much lower 6D space of Aruco Marker pose, the contact location information has been lost [18]. With a much higher dimension of 32 in the SVAE framework, we hypothesize that such information could be maintained in the latent space to a certain degree. A preliminary test was conducted by categorizing the training samples into three contact events: no contact, contact at the finger’s tip, and the middle region. We trained a contact event classifier using the SVAE

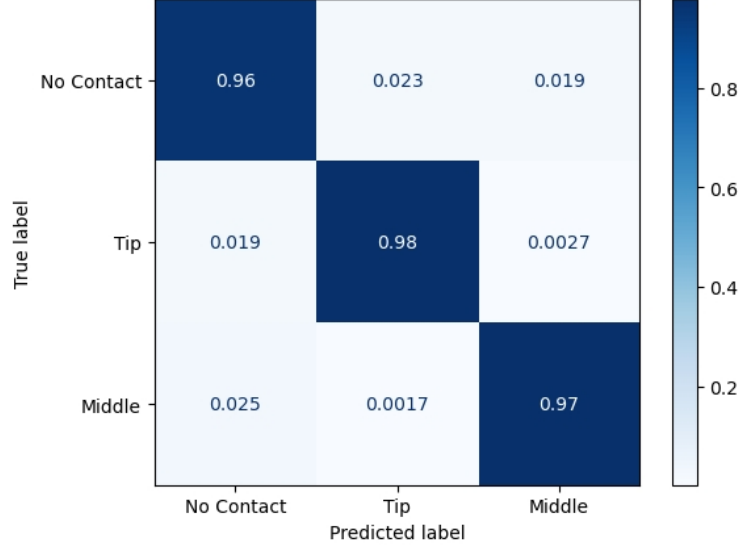


Figure 13: **Confusion matrix of contact event detection.** The tip and middle labels refer to the top and middle regions of the soft polyhedral network during contact.

framework shown in Fig. 7, which can be formulated by

$$\{\mathbf{Event}_{\text{Contact}}, \mathbf{M}^{\text{Gen}}\} = f_3(\text{Dynamic}^{\text{STN}} \mathbf{M}^{\text{Seg}}, \mathbf{M}_{t=0}^{\text{Seg}}), \quad (8)$$

$$f_3 = \text{SVAE}.$$

Figure 13 shows the confusion matrix of the classifier evaluated on the validation dataset of 8,000 samples. The accuracies for all three contact events are above 97%. Considering the classifier only takes the SPN’s mask as input, which filters out all the see-through visual information, the results confirm our hypothesis that the soft touch represented by the latent vectors contains information such as force/torque and contact location. A real-time demonstration is included in the supplementary video. The binary classes of the contact location are partly limited by the data collection process, where the precise locations were not recorded. The granularity could be further improved by using denser labels or by converting it into a regression task.

5 Conclusion, Limitations, and Future Directions

Inspired by sensory substitution from biological agents, this study presents a Vision-based See-Through Perception (VBSeeThruP) approach to reason among different image layers for visual- and contact-based information from a single camera input. By placing a See-Thru-Network in front of a single in-finger camera, two layers of information can be obtained: one at a closer range for the soft interface, awaiting contact interactions, and another about the scene at a distance but occluded. Contact-based perception is substituted markerlessly by reasoning about the masked deformation, facilitating reactive see-through grasping.

Despite encouraging results, there are notable constraints. First, while XMem runs at 30 Hz, it remains significantly slower than the camera’s potential 330 Hz frame rate, and the overall pipeline still needs optimization for high-speed robotic tasks. Second, mislabeled detections sometimes occur because we did not fine-tune object detection for specific targets. Third, the learned 6D force/torque model exhibits a systematic shift when applied to new fingers with slightly different initial templates. Although subtracting this offset mitigates the error, more effective data augmentation strategies could further improve generalization. Finally, larger scenes often appear blurry through the STN, limiting the range of reliable visual perception.

Several directions remain open. Promising avenues include underwater perception and manipulation [77], embodied robot learning with multi-modal feedback that integrates SPN’s omni-directional adaptability and precise 6D force/torque sensing [78], and extending the single-camera approach to stereo vision for improved 3D reconstruction or 6D pose estimation.

Acknowledgement

This work was partly supported by the National Natural Science Foundation of China under Grants 62473189 and 62206119, as well as the Shenzhen Long-Term Support for Higher Education at SUSTech under Grant 20231115141649002.

Author Fang Wan would like to thank Prof. Roberto Calandra and all organizers and participants of the 2024 Touch Sensing and Processing Summer School in Dresden for their valuable discussions and constructive feedback on this work.

Supplementary Materials

Please refer to this link for supplementary videos of this paper.

References

- [1] Paul Bach-y Rita and Stephen W. Kercel. Sensory Substitution and the Human-Machine Interface. *Trends in Cognitive Sciences*, 7(12):541–546, 2003.
- [2] Emilie A. Caspar, Albert De Beir, Pedro A. Magalhaes De Saldanha Da Gama, Florence Yernaux, Axel Cleeremans, and Bram Vanderborght. New frontiers in the Rubber Hand Experiment: When a Robotic Hand Becomes One’s Own. *Behavior Research Methods*, 47(3):744–755, 2015.
- [3] Matthew Botvinick and Jonathan Cohen. Rubber Hands ‘Feel’ Touch That Eyes See. *Nature*, 391(6669):756–756, 1998.
- [4] Manos Tsakiris and Patrick Haggard. The Rubber Hand Illusion Revisited: Visuotactile Integration and Self-attribution. *Journal of Experimental Psychology: Human Perception and Performance*, 31(1):80, 2005.
- [5] Göran Lundborg, Birgitta Rosén, and Styrbjörn Lindberg. Hearing as Substitution for Sensation: A New Principle for Artificial Sensibility. *The Journal of Hand Surgery*, 24(2):219–224, 1999.
- [6] Hang Yin, Anastasia Varava, and Danica Kragic. Modeling, Learning, Perception, and Control Methods for Deformable Object Manipulation. *Science Robotics*, 6(54):eabd8803, 2021.
- [7] Jianhua Li, Siyuan Dong, and Edward Adelson. Slip Detection with Combined Tactile and Visual Information. In *IEEE International Conference on Robotics and Automation (ICRA)*, pages 7772–7777, 2018.
- [8] Alex Alspach, Kunimatsu Hashimoto, Naveen Kuppaswamy, and Russ Tedrake. Soft-Bubble: A Highly Compliant Dense Geometry Tactile Sensor for Robot Manipulation. In *IEEE International Conference on Soft Robotics (RoboSoft)*, pages 597–604, 2019.
- [9] John Lloyd and Nathan F. Lepora. Pose-and-Shear-Based Tactile Servoing. *The International Journal of Robotics Research*, 43(7):1024–1055, 2024.
- [10] Maria Bauza, Antonia Bronars, Yifan Hou, Ian Taylor, Nikhil Chavan-Dafle, and Alberto Rodriguez. SimPLE, a Visuotactile Method Learned in Simulation to Precisely Pick, Localize, Regrasp, and Place Objects. *Science Robotics*, 9(91):eadi8808, 2024.
- [11] Philipp Mittendorf and Gordon Cheng. Humanoid Multimodal Tactile-Sensing Modules. *IEEE Transactions on Robotics*, 27(3):401–410, 2011.
- [12] Mike Lambeta, Tingfan Wu, Ali Sengul, Victoria Rose Most, Nolan Black, Kevin Sawyer, Romeo Mercado, Haozhi Qi, Alexander Sohn, Byron Taylor, Norb Tydingco, Gregg Kammerer, Dave Stroud, Jake Khatha, Kurt Jenkins, Kyle Most, Neal Stein, Ricardo Chavira, Thomas Craven-Bartle, Eric Sanchez, Yitian Ding, Jitendra Malik, and Roberto Calandra. Digitizing Touch with an Artificial Multimodal Fingertip. In *arXiv:2411.02479 [cs.RO]*, 2024.
- [13] Zehang Weng, Peng Zhou, Hang Yin, Alexander Kravberg, Anastasiia Varava, David Navarro-Alarcon, and Danica Kragic. Interactive Perception for Deformable Object Manipulation. *IEEE Robotics and Automation Letters*, 9(9):7763–7770, 2024.
- [14] Jihong Zhu, David Navarro-Alarcon, Robin Passama, and Andrea Cherubini. Vision-based Manipulation of Deformable and Rigid Objects using Subspace Projections of 2D Contours. *Robotics and Autonomous Systems*, 142:103798, 2021.
- [15] N. Fazeli, M. Oller, J. Wu, Z. Wu, J. B. Tenenbaum, and A. Rodriguez. See, Feel, Act: Hierarchical Learning for Complex Manipulation Skills with Multisensory Fusion. *Science Robotics*, 4(26):eaav3123, 2019.

- [16] Huanbo Sun, Katherine J. Kuchenbecker, and Georg Martius. A Soft Thumb-Sized Vision-Based Sensor with Accurate All-Round Force Perception. *Nature Machine Intelligence*, 4(2):135–145, 2022.
- [17] Ning Guo, Xudong Han, Shuqiao Zhong, Zhiyuan Zhou, Jian Lin, Jiansheng Dai, Fang Wan, and Chaoyang Song. Proprioceptive State Estimation for Amphibious Tactile Sensing. *IEEE Transactions on Robotics*, 40:4684–4698, 2024.
- [18] Xiaobo Liu, Xudong Han, Wei Hong, Fang Wan, and Chaoyang Song. Proprioceptive Learning with Soft Polyhedral Networks. *The International Journal of Robotics Research*, 43(12):1916–1935, 2024.
- [19] Alexander Kirillov, Eric Mintun, Nikhila Ravi, Hanzi Mao, Chloe Rolland, Laura Gustafson, Tete Xiao, Spencer Whitehead, Alexander C. Berg, Wan-Yen Lo, Piotr Dollár, and Ross Girshick. Segment Anything. In *arXiv:2304.02643 [cs.CV]*, 2023.
- [20] Nicole Robinson, Brendan Tidd, Dylan Campbell, Dana Kulić, and Peter Corke. Robotic Vision for Human-Robot Interaction and Collaboration: A Survey and Systematic Review. *ACM Transactions on Human-Robot Interaction*, 12(1), 2023.
- [21] Shoujie Li, Haixin Yu, Guoping Pan, Huaze Tang, Jiawei Zhang, Linqi Ye, Xiao-Ping Zhang, and Wenbo Ding. M³Tac: A Multispectral Multimodal Visuotactile Sensor With Beyond-Human Sensory Capabilities. *IEEE Transactions on Robotics*, 40:4506–4525, 2024.
- [22] Can Zhao, Jin Liu, and Daolin Ma. iFEM2.0: Dense 3-D Contact Force Field Reconstruction and Assessment for Vision-Based Tactile Sensors. *IEEE Transactions on Robotics*, 41:289–305, 2025.
- [23] Oliver Kroemer, Scott Niekum, and George Konidaris. A Review of Robot Learning for Manipulation: Challenges, Representations, and Algorithms. *Journal of Machine Learning Research*, 22(30):1–82, 2021.
- [24] Shaoqing Ren, Kaiming He, Ross Girshick, and Jian Sun. Faster R-CNN: Towards Real-Time Object Detection with Region Proposal Networks. *IEEE Transactions on Pattern Analysis and Machine Intelligence*, 39(6):1137–1149, 2017.
- [25] Joseph Redmon, Santosh Divvala, Ross Girshick, and Ali Farhadi. You Only Look Once: Unified, Real-Time Object Detection. In *IEEE/CVF Conference on Computer Vision and Pattern Recognition (CVPR)*, pages 779–788, 2016.
- [26] Vincent Lepetit, Francesc Moreno-Noguer, and Pascal Fua. EPnP: An Accurate O(n) Solution to the PnP Problem. *International Journal of Computer Vision*, 81(2):155–166, 2009.
- [27] P.J. Besl and Neil D. McKay. A Method for Registration of 3-D Shapes. *IEEE Transactions on Pattern Analysis and Machine Intelligence*, 14(2):239–256, 1992.
- [28] Jeannette Bohg, Antonio Morales, Tamim Asfour, and Danica Kragic. Data-Driven Grasp Synthesis - A Survey. *IEEE Transactions on Robotics*, 30(2):289–309, 2014.
- [29] Veronica E. Arriola-Rios, Puren Guler, Fanny Ficuciello, Danica Kragic, Bruno Siciliano, and Jeremy L. Wyatt. Modeling of Deformable Objects for Robotic Manipulation: A Tutorial and Review. *Frontiers in Robotics and AI*, 7, 2020.
- [30] Oliver Kroemer, Christoph H. Lampert, and Jan Peters. Learning Dynamic Tactile Sensing With Robust Vision-Based Training. *IEEE Transactions on Robotics*, 27(3):545–557, 2011.
- [31] Jihong Zhu, Andrea Cherubini, Claire Dune, David Navarro-Alarcon, Farshid Alambeigi, Dmitry Berenson, Fanny Ficuciello, Kensuke Harada, Jens Kober, Xiang Li, Jia Pan, Wenzhen Yuan, and Michael Gienger. Challenges and Outlook in Robotic Manipulation of Deformable Objects. *IEEE Robotics & Automation Magazine*, 29(3):67–77, 2022.
- [32] Yuhong Deng and David Hsu. General-Purpose Clothes Manipulation with Semantic Keypoints. In *arXiv:2408.08160 [cs.RO]*, 2024.
- [33] Quan Khanh Luu, Nhan Huu Nguyen, and Van Anh Ho. Simulation, Learning, and Application of Vision-Based Tactile Sensing at Large Scale. *IEEE Transactions on Robotics*, 39(3):2003–2019, 2023.
- [34] Ning Guo, Xudong Han, Shuqiao Zhong, Zhiyuan Zhou, Jian Lin, Fang Wan, and Chaoyang Song. Reconstructing Soft Robotic Touch via In-Finger Vision. *Advanced Intelligent Systems*, 6(10):2400022, 2024.
- [35] Wenzhen Yuan, Siyuan Dong, and Edward H. Adelson. GelSight: High-Resolution Robot Tactile Sensors for Estimating Geometry and Force. *Sensors*, 17(12), 2017.
- [36] Shaoxiong Wang, Mike Lambeta, Po-Wei Chou, and Roberto Calandra. TACTO: A Fast, Flexible, and Open-Source Simulator for High-Resolution Vision-Based Tactile Sensors. *IEEE Robotics and Automation Letters*, 7(2):3930–3937, 2022.

- [37] Sandra Q. Liu and Edward H. Adelson. GelSight Fin Ray: Incorporating Tactile Sensing into a Soft Compliant Robotic Gripper. In *IEEE International Conference on Soft Robotics (RoboSoft)*, pages 925–931, 2022.
- [38] Jialiang Zhao and Edward H. Adelson. GelSight Svelte: A Human Finger-Shaped Single-Camera Tactile Robot Finger with Large Sensing Coverage and Proprioceptive Sensing. In *IEEE/RSJ International Conference on Intelligent Robots and Systems (IROS)*, pages 8979–8984, 2023.
- [39] Teresa A Kent, Suhan Kim, Gabriel Kornilowicz, Wenzhen Yuan, Mitra J. Z. Hartmann, and Sarah Bergbreiter. WhiskSight: A Reconfigurable, Vision-Based, Optical Whisker Sensing Array for Simultaneous Contact, Airflow, and Inertia Stimulus Detection. *IEEE Robotics and Automation Letters*, 6(2):3357–3364, 2021.
- [40] Francois R. Hogan, Jean-François Tremblay, Bobak H. Baghi, Michael Jenkin, Kaleem Siddiqi, and Gregory Dudek. Finger-STs: Combined Proximity and Tactile Sensing for Robotic Manipulation. *IEEE Robotics and Automation Letters*, 7(4):10865–10872, 2022.
- [41] Yazhan Zhang, Weihao Yuan, Zicheng Kan, and Michael Yu Wang. Towards Learning to Detect and Predict Contact Events on Vision-based Tactile Sensors. In Leslie Pack Kaelbling, Danica Kragic, and Komei Sugiura, editors, *Proceedings of the Conference on Robot Learning*, volume 100 of *Proceedings of Machine Learning Research*, pages 1395–1404. PMLR, 30 Oct–01 Nov 2020.
- [42] Wenzhen Yuan, Shaoxiong Wang, Siyuan Dong, and Edward Adelson. Connecting Look and Feel: Associating the Visual and Tactile Properties of Physical Materials. In *IEEE Conference on Computer Vision and Pattern Recognition (CVPR)*, July 2017.
- [43] Weiliang Xu, Guoyuan Zhou, Yuanzhi Zhou, Zhibin Zou, Jiali Wang, Wenfeng Wu, and Xinming Li. A Vision-Based Tactile Sensing System for Multimodal Contact Information Perception via Neural Network. *IEEE Transactions on Instrumentation and Measurement*, 73:1–11, 2024.
- [44] Lac Van Duong and Van Anh Ho. Large-Scale Vision-Based Tactile Sensing for Robot Links: Design, Modeling, and Evaluation. *IEEE Transactions on Robotics*, 37(2):390–403, 2021.
- [45] Qiang Zhang, Yunzhu Li, Yiyue Luo, Wan Shou, Michael Foshey, Junchi Yan, Joshua B. Tenenbaum, Wojciech Matusik, and Antonio Torralba. Dynamic Modeling of Hand-Object Interactions via Tactile Sensing. In *IEEE/RSJ International Conference on Intelligent Robots and Systems (IROS)*, pages 2874–2881, 2021.
- [46] Qiang Li, Oliver Kroemer, Zhe Su, Filipe Fernandes Veiga, Mohsen Kaboli, and Helge Joachim Ritter. A Review of Tactile Information: Perception and Action Through Touch. *IEEE Transactions on Robotics*, 36(6):1619–1634, 2020.
- [47] Sami Haddadin, Lars Johannsmeier, and Fernando Díaz Ledezma. Tactile Robots as a Central Embodiment of the Tactile Internet. *Proceedings of the IEEE*, 107(2):471–487, 2019.
- [48] Pietro Falco, Shuang Lu, Andrea Cirillo, Ciro Natale, Salvatore Pirozzi, and Dongheui Lee. Cross-Modal Visuo-Tactile Object Recognition using Robotic Active Exploration. In *IEEE International Conference on Robotics and Automation (ICRA)*, pages 5273–5280, 2017.
- [49] Prajval Kumar Murali, Bernd Porr, and Mohsen Kaboli. Shared Visuo-Tactile Interactive Perception for Robust Object Pose Estimation. *The International Journal of Robotics Research*, page 02783649241301443, 2024.
- [50] Sudharshan Suresh, Haozhi Qi, Tingfan Wu, Taosha Fan, Luis Pineda, Mike Lambeta, Jitendra Malik, Mrinal Kalakrishnan, Roberto Calandra, Michael Kaess, Joseph Ortiz, and Mustafa Mukadam. NeuralFeels with neural fields: Visuotactile perception for in-hand manipulation. *Science Robotics*, 9(96):eadl0628, 2024.
- [51] Anirvan Dutta, Etienne Burdet, and Mohsen Kaboli. Predictive Visuo-Tactile Interactive Perception Framework for Object Properties Inference. *IEEE Transactions on Robotics*, 2025.
- [52] Nicolás Navarro-Guerrero, Sibel Toprak, Josip Josifovski, and Lorenzo Jamone. Visuo-Haptic Object Perception for Robots: An Overview. *Autonomous Robots*, 47(4):377–403, 2023.
- [53] Alessandro Pieropan, Giampiero Salvi, Karl Pauwels, and Hedvig Kjellström. Audio-Visual Classification and Detection of Human Manipulation Actions. In *IEEE/RSJ International Conference on Intelligent Robots and Systems (IROS)*, pages 3045–3052, 2014.
- [54] Mariella Dimiccoli, Shubhan Patni, Matej Hoffmann, and Francesc Moreno-Noguer. Recognizing Object Surface Material from Impact Sounds for Robot Manipulation. In *IEEE/RSJ International Conference on Intelligent Robots and Systems (IROS)*, pages 9280–9287, 2022.
- [55] Hao Li, Yizhi Zhang, Junzhe Zhu, Shaoxiong Wang, Michelle A Lee, Huazhe Xu, Edward Adelson, Li Fei-Fei, Ruohan Gao, and Jiajun Wu. See, Hear, and Feel: Smart Sensory Fusion for Robotic Manipulation. In Karen Liu, Dana Kulic, and Jeff Chnowski, editors, *Proceedings of The 6th Conference on Robot Learning*, volume 205 of *Proceedings of Machine Learning Research*, pages 1368–1378, 14–18 Dec 2023.

- [56] Zhongli Wang, Guohui Tian, and Hao Pan. Robot Gaining Robust Pouring Skills Through Fusing Vision and Audio. *ISA transactions*, 135:428–437, 2023.
- [57] Xiaoqi Li, Mingxu Zhang, Yiran Geng, Haoran Geng, Yuxing Long, Yan Shen, Renrui Zhang, Jiaming Liu, and Hao Dong. ManipLLM: Embodied Multimodal Large Language Model for Object-Centric Robotic Manipulation. In *IEEE/CVF Conference on Computer Vision and Pattern Recognition (CVPR)*, pages 18061–18070, 2024.
- [58] Yunfan Jiang, Agrim Gupta, Zichen Zhang, Guanzhi Wang, Yongqiang Dou, Yanjun Chen, Li Fei-Fei, Anima Anandkumar, Yuke Zhu, and Linxi Fan. VIMA: Robot Manipulation with Multimodal Prompts. In *International Conference on Machine Learning (ICML)*, volume 202, pages 14975–15022, 23–29 Jul 2023.
- [59] Wenqiang Lai, Tianwei Zhang, Tin Lun Lam, and Yuan Gao. Vision-Language Model-based Physical Reasoning for Robot Liquid Perception. In *IEEE/RSJ International Conference on Intelligent Robots and Systems (IROS)*, pages 9652–9659, 2024.
- [60] Danny Driess, Fei Xia, Mehdi S. M. Sajjadi, Corey Lynch, Aakanksha Chowdhery, Brian Ichter, Ayzaan Wahid, Jonathan Tompson, Quan Vuong, Tianhe Yu, Wenlong Huang, Yevgen Chebotar, Pierre Sermanet, Daniel Duckworth, Sergey Levine, Vincent Vanhoucke, Karol Hausman, Marc Toussaint, Klaus Greff, Andy Zeng, Igor Mordatch, and Pete Florence. PaLM-E: An Embodied Multimodal Language Model. In *International Conference on Machine Learning (ICML)*, volume 202, pages 8469–8488, 2023.
- [61] Jiaming Liu, Mengzhen Liu, Zhenyu Wang, Pengju An, Xiaoqi Li, Kaichen Zhou, Senqiao Yang, Renrui Zhang, Yandong Guo, and Shanghang Zhang. RoboMamba: Efficient Vision-Language-Action Model for Robotic Reasoning and Manipulation. In *arXiv:2406.04339 [cs.CV]*, 2024.
- [62] Fang Wan, Haokun Wang, Xiaobo Liu, Linhan Yang, and Chaoyang Song. DeepClaw: A Robotic Hardware Benchmarking Platform for Learning Object Manipulation. In *IEEE/ASME International Conference on Advanced Intelligent Mechatronics (AIM)*, pages 2011–2018, 2020.
- [63] Fang Wan, Xiaobo Liu, Ning Guo, Xudong Han, Feng Tian, and Chaoyang Song. Visual Learning towards Soft Robot Force Control using a 3D Metamaterial with Differential Stiffness. In Aleksandra Faust, David Hsu, and Gerhard Neumann, editors, *Conference on Robot Learning (CoRL)*, volume 164 of *Proceedings of Machine Learning Research*, pages 1269–1278. PMLR, 08–11 Nov 2022.
- [64] Berk Calli, Arjun Singh, Aaron Walsman, Siddhartha Srinivasa, Pieter Abbeel, and Aaron M. Dollar. The YCB Object and Model set: Towards Common Benchmarks for Manipulation Research. In *International Conference on Advanced Robotics (ICAR)*, pages 510–517, 2015.
- [65] Ho Kei Cheng and Alexander G Schwing. XMem: Long-Term Video Object Segmentation with an Atkinson-Shiffrin Memory Model. In *European Conference on Computer Vision (ECCV)*, 2022.
- [66] F. Perazzi, J. Pont-Tuset, B. McWilliams, L. Van Gool, M. Gross, and A. Sorkine-Hornung. A Benchmark Dataset and Evaluation Methodology for Video Object Segmentation. In *IEEE Conference on Computer Vision and Pattern Recognition (CVPR)*, pages 724–732, 2016.
- [67] Weize Quan, Jiayi Chen, Yanli Liu, Dong-Ming Yan, and Peter Wonka. Deep Learning-Based Image and Video Inpainting: A Survey. *International Journal of Computer Vision*, 132(7):2367–2400, 2024.
- [68] Zhen Li, Cheng-Ze Lu, Jianhua Qin, Chun-Le Guo, and Ming-Ming Cheng. Towards An End-to-End Framework for Flow-Guided Video Inpainting. In *IEEE/CVF Conference on Computer Vision and Pattern Recognition (CVPR)*, pages 17541–17550, 2022.
- [69] Yian Zhao, Wenyu Lv, Shangliang Xu, Jinman Wei, Guanzhong Wang, Qingqing Dang, Yi Liu, and Jie Chen. DETRs Beat YOLOs on Real-time Object Detection. In *IEEE/CVF Conference on Computer Vision and Pattern Recognition (CVPR)*, pages 16965–16974, 2024.
- [70] Glenn Jocher, Jing Qiu, and Ayush Chaurasia. Ultralytics YOLO, January 2024.
- [71] Lihe Yang, Bingyi Kang, Zilong Huang, Zhen Zhao, Xiaogang Xu, Jiashi Feng, and Hengshuang Zhao. Depth Anything V2. In *arXiv:2406.09414 [cs.CV]*, 2024.
- [72] Nikhila Ravi, Valentin Gabeur, Yuan-Ting Hu, Ronghang Hu, Chaitanya Ryali, Tengyu Ma, Haitham Khedr, Roman Rädle, Chloe Rolland, Laura Gustafson, Eric Mintun, Junting Pan, Kalyan Vasudev Alwala, Nicolas Carion, Chao-Yuan Wu, Ross Girshick, Piotr Dollár, and Christoph Feichtenhofer. SAM 2: Segment Anything in Images and Videos. In *arXiv:2408.00714 [cs.CV]*, 2024.
- [73] Akihiko Yamaguchi and Christopher G. Atkeson. Combining Finger Vision and Optical Tactile Sensing: Reducing and Handling Errors while Cutting Vegetables. In *IEEE-RAS 16th International Conference on Humanoid Robots (Humanoids)*, pages 1045–1051, 2016.

- [74] Mike Lambeta, Po-Wei Chou, Stephen Tian, Brian Yang, Benjamin Maloon, Victoria Rose Most, Dave Stroud, Raymond Santos, Ahmad Byagowi, Gregg Kammerer, Dinesh Jayaraman, and Roberto Calandra. DIGIT: A Novel Design for a Low-Cost Compact High-Resolution Tactile Sensor With Application to In-Hand Manipulation. *IEEE Robotics and Automation Letters*, 5(3):3838–3845, 2020.
- [75] Nathan F. Lepora. Soft Biomimetic Optical Tactile Sensing With the TacTip: A Review. *IEEE Sensors Journal*, 21(19):21131–21143, 2021.
- [76] Wen Fan, Haoran Li, Weiyong Si, Shan Luo, Nathan Lepora, and Dandan Zhang. ViTacTip: Design and Verification of a Novel Biomimetic Physical Vision-Tactile Fusion Sensor. In *arXiv:2402.00199 [cs.RO]*, 2024.
- [77] Oussama Khatib, Xiyang Yeh, Gerald Brantner, Brian Soe, Boyeon Kim, Shameek Ganguly, Hannah Stuart, Shiquan Wang, Mark Cutkosky, Aaron Edsinger, Phillip Mullins, Mitchell Barham, Christian R. Woolstra, Khaled Nabil Salama, Michel L’Hour, and Vincent Creuze. Ocean One: A Robotic Avatar for Oceanic Discovery. *IEEE Robotics and Automation Magazine*, 23(4):20–29, 2016.
- [78] Cheng Chi, Zhenjia Xu, Chuer Pan, Eric Cousineau, Benjamin Burchfiel, Siyuan Feng, Russ Tedrake, and Shuran Song. Universal Manipulation Interface: In-The-Wild Robot Teaching Without In-The-Wild Robots. In *Proceedings of Robotics: Science and Systems (RSS)*, 2024.